



RESEARCH MEMORANDUM

INVESTIGATION OF AN EXPERIMENTAL SUPERSONIC
AXIAL-FLOW COMPRESSOR

By

John R. Erwin, Linwood C. Wright,
and Arthur Kantrowitz

Langley Memorial Aeronautical Laboratory
Langley Field, Va.

~~CONFIDENTIAL~~

This document contains classified information affecting the National Defense of the United States within the meaning of the Espionage Act, USC 50:31 and 32. Its transmission or the revelation of its contents in any manner to an unauthorized person is prohibited by law. Information so classified may be imparted only to persons in the military and naval services of the United States, appropriate civilian officers and employees of the Federal Government who have a legitimate interest therein, and to United States citizens of known loyalty and discretion who of necessity must be informed thereof.

AMDC
LIBRARY
2011

NATIONAL ADVISORY COMMITTEE FOR AERONAUTICS

WASHINGTON
August 7, 1947

RML 501b

7067

[Handwritten signature]



NATIONAL ADVISORY COMMITTEE FOR AERONAUTICS

RESEARCH MEMORANDUM

INVESTIGATION OF AN EXPERIMENTAL SUPERSONIC
AXIAL-FLOW COMPRESSOR

By John R. Erwin, Linwood C. Wright,
and Arthur Kantrowitz

SUMMARY

As a part of an investigation that is being conducted to explore the possibilities of axial-flow compressors operating with supersonic velocities relative to the blading, a preliminary experimental investigation has been made of a supersonic compressor designed to produce a high pressure ratio in a single stage.

The compressor was designed for a pressure ratio of 2.9 on the basis of the theory of a supersonic flow entering a cascade and the diffusion efficiencies obtained experimentally in 1-inch-jet tests of static models. No significant departures from the theory of the entrance flow into a supersonic cascade were found, but the efficiency of diffusion in the rotor was found to be considerably lower than that obtained in the 1-inch-jet experiments. A complete explanation of this discrepancy has not yet been obtained, but the numerous structural inaccuracies of this rotor contributed significantly to this effect, as was shown by a few preliminary tests of an accurately constructed rotor.

Freon-12 was used as the testing medium to reduce structural problems. The mass flow measured for the 16-inch-diameter rotor, about 28.5 pounds per second when converted to sea-level air, agreed with theoretical expectations. Flow conditions leaving the rotor were obtained by surveys. A pressure ratio of about 1.8 with 83 percent rotor efficiency was measured. If a 90-percent dynamic-pressure recovery in the stators were assumed, this efficiency would be reduced about 3 percent.

The supersonic compressor shows promise of being more compact by a factor of about 4 than any comparable machine performing the same operation. Inasmuch as the experimental machine must be regarded as very primitive and many opportunities for important improvements exist, supersonic compressors are considered to have great promise, especially for the design of high-performance turbojets.

*Unclassified
by Authority of
NASA
No further dissemination
without necessary
approval in
July 1980 - J.R.E.*

INTRODUCTION

An investigation is in progress at the Langley Laboratory of the NACA to explore the possibilities of axial-flow compressors operating with supersonic velocities relative to the blade rows. The first phase of this investigation, a study of supersonic diffusers, has been reported in reference 1. The second phase, an analysis of supersonic compressors, has been reported in reference 2. Preliminary calculations have shown that very high pressure ratios across a stage, together with somewhat increased mass flows, are possible with compressors which decelerate air through the speed of sound in their rotor blading. These performance characteristics are desirable in compressors for aircraft jet-propulsion units, gas turbines, or superchargers. The third phase, presented herein, is a preliminary experimental investigation of a supersonic compressor designed to produce a high pressure ratio in a single stage.

It is commonly supposed that flow at speeds higher than the speed of sound necessarily involves large energy losses. The first two phases of this investigation, which have been reported in references 1 and 2, were primarily concerned with the magnitude of these losses. It has been demonstrated theoretically (reference 2) that the waves which are primarily responsible for the high drag of isolated bodies at supersonic speeds can be entirely eliminated in the case of a cascade. It is important that any normal shock existing be everywhere confined by the blading. Theoretical results indicated that, in cases where the normal shock is not confined, large losses due to a wave system extending far from the cascade can result. The other source of large losses is that accompanying the confined normal shock which decelerates air through the speed of sound. In order to study the magnitude of these losses, the preliminary investigation of supersonic diffusers was undertaken. It was found possible to design supersonic diffusers to decelerate air from Mach numbers up to 2 through the speed of sound with efficiencies comparable with those obtained with good subsonic diffusers. These two preliminary investigations have indicated no cause for the efficiency of supersonic compressors to be necessarily low. Because of these encouraging results, tests were made of an experimental supersonic compressor at the Langley Laboratory of the NACA.

The general object of this investigation was to verify the performance indicated for such compressors by simplified theory. In particular, it was desired to determine several indicated characteristics of operation: (1) whether reasonable efficiencies could be obtained with a compressor operating with a normal shock confined within the rotor passages, (2) whether the very high

pressure rises predicted could be obtained, and (3) whether the simplified theory of the supersonic entrance region was valid.

Of the many possibilities for supersonic compressors, three elementary single-stage designs, all having subsonic axial velocities, were discussed in reference 2. For preliminary experiments, a single-stage compressor similar to design 2 of reference 2 and having an entering Mach number of 1.6 relative to the blades and deceleration of the flow velocities through the speed of sound in the rotor blades was selected. This type of compressor offered, with a minimum of development, a significant increase in the pressure rise available from a single stage.

In order to develop blade profiles, two- and three-dimensional models of a single passage were studied in a 1-inch jet. Pressure-distribution methods and schlieren methods were employed. The performance of these static models was used as a basis for alteration of the compressor tested.

In order to reduce structural and power requirements, the compressor was tested in Freon-12 at low pressure. Performance measurements were taken at several tip speeds ranging from 70 to 160 percent of the initial speed of sound.

SYMBOLS

a	velocity of sound, feet per second
A	area, square feet
A_{disk}	area of rotor disk, square feet
E_R	expansion ratio (A_1/A_2) (fig. 6)
C_R	contraction ratio (A_2/A_3) (fig. 6)
C_G	mass-flow coefficient $\left(\frac{G}{\rho_{cr} a_{cr} A_{\text{disk}}} \right)$
c_p	specific heat at constant pressure, foot pounds per slug per °F
g	acceleration due to gravity, 32.2 feet per second ²
M	Mach number, ratio of flow velocity to the velocity of sound (V/a)
M_c	compressor Mach number (U_t/a_0)

L

G

$$\text{mass flow} \left(2\pi \int_{r_h}^{r_t} \rho V \cos \theta r dr \right)$$

dG

differential mass flow $(2\pi \rho V \cos \theta r dr)$

N

rotational speed of rotor, revolutions per minute

P

total pressure, atmospheres

p

static pressure, atmospheres

r

radius, feet

R

gas constant, foot pounds per slug per °F

R_m

gas constant for mixture of Freon-12 and air, foot pounds per slug per °F

T

temperature, °F absolute

ΔT

thermocouple stagnation temperature rise

ΔT'

adiabatic stagnation temperature rise

$$\left(T_0 \left(\frac{P_5}{P_0} \right)^{R_m/c_p} - T_0 \right)$$

$$\Delta T'_{wt} = \frac{\int_{r_h}^{r_t} \Delta T' dG_5}{G_5}$$

U

rotational velocity of blade element at any radius, feet per second (fig. 2)

V

velocity of fluid, stationary coordinates, feet per second (fig. 2)

W

velocity of fluid relative to rotor, feet per second (fig. 2)

β

angle between axial direction and entering-flow direction in rotor coordinates, degrees (fig. 2)

δ

turning angle, rotor coordinates, degrees (fig. 2)

η_r rotor efficiency, evaluated from survey over rotor blade annulus

$$\left(\frac{\int_{r_h}^{r_t} c_p \Delta T' dG_5}{\int_{r_h}^{r_t} U_5 V_{5 \tan} dG_5 - \int_{r_h}^{r_t} U_1 V_{1 \tan} dG_1} \right)$$

γ ratio of specific heats

θ angle between flow direction and axial direction in stationary coordinates, degrees (fig. 2)

ρ density, slugs per cubic foot

σ solidity $\left(\frac{\text{Blade chord}}{\text{Blade spacing}} \right)$

Subscripts:

a axial direction

av average

cr critical condition (velocity of sound when $M = 1$)

h root diameter

p pitch diameter

t tip diameter

tan tangential direction

s stagnation

o initial stagnation conditions

1 rotor entrance, stationary coordinates

2 rotor entrance, rotor coordinates, or 1-inch-jet-model entrance

3 blade minimum area, rotor coordinates

4 rotor exit, rotor coordinates, or 1-inch-jet-model exit

5 rotor exit, stationary coordinates

wt average value weighted on basis of mass flow

GENERAL AERODYNAMIC DESIGN

Although the compressor used for the present study was intended primarily for experimental purposes, it was thought desirable in selecting the design conditions to choose values that would permit the development of a machine having practical applications with a minimum of effort in the event that the results warrant such a development. A small high-performance compressor was therefore designed from the following specifications:

(1) The highest rotational velocity currently being used for aircraft gas turbines, 1600 feet per second at the tip diameter, was adopted for aerodynamic design purposes (compressor Mach number $M_c = 1.43$).

(2) An axial Mach number of about 0.80 entering the rotor at the pitch diameter was selected. This value permitted the use of guide vanes without local supersonic velocities. The mass flow at $M = 0.80$ is only about 3.7 percent below the maximum that would occur with sonic velocity.

(3) Guide vanes were used to aid in the establishment of equilibrium conditions as mentioned subsequently; the turning angles selected were only a few degrees from the axial direction. This arrangement reduced the mass flow only slightly, about 1 percent below that which would be obtained with axial flow.

(4) The deceleration and turning in the rotor blading were limited by the subsonic stator critical-speed considerations. These limiting values were accepted as the basis of the rotor blade design.

(5) A value of r_h/r_t of 0.75 was selected.

The first three conditions determined the Mach number, $M = 1.6$, relative to the rotating blades at the pitch diameter, and the stagger angle, $\beta = 60^\circ$. The fifth condition largely determined the design mass flow of about 30 pounds per second for the 16-inch-diameter rotor, with stationary sea-level atmospheric entry.

During the period of the design of this compressor, the establishment of certain flow conditions was held to be conducive to the best efficiency. Some of these considerations are now viewed as refinements that might be applied to highly developed supersonic compressors and were abandoned in the present machine in the efforts to reduce separation. Entrance flow into the rotor

was so regulated that the pressure rise experienced through the normal shock would be equal to that required for equilibrium after a theoretical normal shock at all diameters. This condition resulted in almost constant values of Mach number and total pressure entering the rotor at all diameters. Because of the thin blading used in this design, it was decided for structural reasons to make the spanwise blade elements radial. This consideration determined the twist of the blading.

In reference 2, it was shown that for a two-dimensional supersonic cascade the flow enters parallel to the entrance region of the cascade. For a three-dimensional cascade, however, it is possible to have compression waves originating at the tip neutralized by expansion waves from the root, or vice versa. It was decided to avoid these three-dimensional extended wave patterns in these preliminary experiments by producing flow parallel to the entrance region of the blades at the root, pitch, and tip. The design of the guide vanes and the curved entrance passage, as shown in figure 1, were determined by these considerations. An attempt was made to regulate the flow from the rotor so that the total pressures entering the stator root, pitch, and tip would not vary too widely. This requirement necessitated an outward curvature of the rotor passages. (See fig. 1.)

Preliminary velocity diagrams (fig. 2(a)) were developed on the basis of these considerations. These velocity diagrams were chosen from an analysis of possible designs on the basis of the performance of compressor blade models in rough preliminary 1-inch-jet tests. (Velocity diagrams obtained from a second series of 1-inch-jet tests and from tests of the compressor are shown in figs. 2(b), 2(c), and 2(d) for comparison.)

EXPERIMENTAL ROTOR-BLADE DEVELOPMENT

General Considerations

The compressor was designed on the basis of rough preliminary tests in the 1-inch jet and was first tested with the outward curvature of the rotor shroud. The preliminary tests in the 1-inch jet were later found to be invalid and, therefore, the results are not presented. A very low pressure rise and efficiency were obtained in the first compressor tests due to a region of separation covering the outer half of the discharge annulus. It became obvious that improvements in the shape of the rotor-blade passages would be necessary to obtain acceptable performance. A second group of tests of a series of models was made in an attempt to develop satisfactory passages for the supersonic compressor rotor.

As in subsonic compressor investigations, it is convenient to study supersonic compressor blading with static models which can be made and tested easily. Models to provide pressure-distribution data and models to study flow conditions by the schlieren method were tested in the 1-inch jet (fig. 3). These tests were intended as a study of the supersonic operating condition only. An extended cascade would be required to set up the complex wave patterns which would occur in the transonic region. (See fig. 4 of reference 2.) For this reason, all 1-inch-jet tests were made at the design Mach. number relative to the blades of about 1.60.

In order that valid results be obtained from stationary model studies, test conditions must be similar to conditions of compressor operation. In reference 2, it was shown that for the case of the straight entrance region and subsonic axial velocity, no waves move upstream of the rotating cascade in the steady state. For this condition, then, adjacent passages between the blades have no influence on each other and in order to simulate the flow in the blading of a supersonic compressor, it is necessary to simulate only a single passage. However, difficulties in the determination of the "spill" point (see following section) may lead to the use of several passages in this type of testing.

According to the theory of reference 2, for a straight entrance region, the flow enters the cascade parallel to the rearward side of the blade at the leading edge. It would be expected that the pressure at this point would be the same as the pressure upstream from the cascade. In the tests described subsequently, the angle of the model was adjusted to produce this condition.

It is, of course, impossible in a stationary experiment to simulate the boundary-layer conditions entering the blading of a rotating machine. It would be expected that, in a compressor of the type considered in the present study, the boundary layer on the inner and outer casings at the entrance to the rotor would be very thin. For these first tests, therefore, an attempt was made to make the boundary layer entering the passage as thin as possible. The pressure-distribution models were made to start without any initial boundary layer and the schlieren models were made to have as little boundary layer as possible on the glass sides and no initial boundary layer on the blade surfaces.

Pressure-Distribution Tests

Methods and parameters. - A second series of three-dimensional models were studied in the 1-inch jet to develop blading to be used as a basis for altering the blades of the compressor being

investigated. The operation of the rotor blades, as required by the compressor design, was to diffuse the flow from the entering Mach number, $M = 1.6$, and stagger angle, $\beta = 60^\circ$, to an exit Mach number of about $M = 0.60$ while turning the flow about 8.8° . The models represented the profile of the rotor blades at the pitch diameter. A typical model is shown in figure 4.

An exploded view of the 1-inch jet-test setup is shown in figure 3. The pressure at the exit of the model was controlled by the gate valve. A total-pressure survey was made of the model exit by use of a rake of three tubes. The survey apparatus was crude as it was intended only to give rough comparisons. Both sides and the top and bottom of the models were equipped with static-pressure tubes.

Since the flow entering the model is supersonic, no effect due to throttling would be observed outside the model until the back pressure had been increased sufficiently to force the shock outside the model passage. This condition of back pressure, termed the "spill" point, was assumed to be the equivalent of stall in the rotating machine in the supersonic operating range. This spill point was indicated by a change in the pressure measured by a total-pressure tube located outside the passage, as shown in figure 4. A typical plot of the difference between the settling-chamber total pressure and the spill-tube total pressure against throttle setting is shown in figure 5. The location of the spill point is shown in this figure. Pressure distributions and surveys were taken as near as possible to the spill point without actually reaching it, as this point would be expected to be the condition of minimum shock losses and most efficient operation. The supersonic design condition is reached just before throttling produces spill in the model or stall in the compressor.

The total pressure recovered and the exit Mach number were used to evaluate the performance of the model. The pressure recovery was found by actual total-pressure measurements and was also calculated from the expansion ratio E_R , the static-pressure measurements, p_2 and p_4 , the entering pressure ratio p_2/p_0 , and the original stagnation conditions, by the formula

$$P_4 = p_4 \left[\frac{1 + \sqrt{1 + 4 \left(\frac{p_2}{p_4 E_R} \right)^2 \left(\frac{T_{2s}}{T_2} \right) \left(\frac{T_{2s}}{T_2} - 1 \right)}}{2} \right]^{c_p/R}$$

which is derived in appendix A. It can be shown that calculated total pressures are correct only when the total pressure is uniform over the entire exit area. If there is variation, the calculated value would always be low. On the other hand, it is believed that the total-pressure surveys with the three-tube rake give too high an average since no total-pressure tubes were situated deep in the boundary layer. Thus, the actual total pressure lies between the upper value given by the measured total pressure and the lower value given by the calculated total pressure.

The pressure model for which results are presented was tested with two values of the contraction ratio of the supersonic flow region C_R and several values of the expansion ratio of the subsonic region E_R . Most of the expansion occurred as a result of the turning of the blades, which was constant at 8.8° for this series of tests. The expansion was varied by building up or reducing the upper surface of the model. (See fig. 4.) The expansion in the compressor blading was varied similarly, as will be discussed subsequently. A wedge was attached to the rearward side of the blade to increase the contraction ratio (fig. 6). The maximum thickness of this wedge was 0.016 inch tapered to zero at the trailing edge. A typical survey obtained in a test of a model having a contraction ratio $C_R = 1.042$ and an expansion ratio $E_R = 1.12$ is presented in figure 7(a). From the contours of total-pressure recovery (exit total pressure divided by chamber pressure), it is evident that some separation occurred. With an increase in expansion ratio to $E_R = 1.325$ (fig. 7(b)), the separated region increased in area and severity.

Performance. - The measured values of total-pressure recovery and exit Mach number are presented in figure 8. Because the separated region became larger as the expansion ratio was increased, a lower total pressure was recovered. Similarly, the effective expansion ratio was reduced by the separation when the actual expansion ratio was increased beyond a value of about 1.15, and a higher exit Mach number was obtained. With blades of the solidity used, $\sigma = 2.3$, a minimum exit Mach number of 0.60 was obtained.

As in the case of three-dimensional supersonic diffusers, an increase in contraction ratio increases the shock efficiency and consequently the total-pressure recovery. The use of contraction ratios close to the maximum possible for the design Mach number appears also to be desirable structurally since it would lead to thicker blades. A possible disadvantage of this method of increasing efficiency, however, would be in an increase in starting Mach number (lowest Mach number at which supersonic flow will enter the passage) and in discontinuities of performance in the transonic range.

The 1-inch-jet tests indicated the following tentative criterions for design of supersonic-compressor blades: (1) the expansion ratio for a solidity of 2.3 could not be greater than about 1.12 without separation - this rate of expansion is approximately equivalent to that of a 40° conical diffuser; (2) a contraction ratio of 1.092 was not excessive for a free-stream Mach number of 1.58 in air.

Schlieren Tests

The general arrangement for taking schlieren photographs of the flow through a typical model (fig. 9) was similar to that used in tests of the pressure-distribution model. The model passage was curved to represent the original design pitch section. The expansion ratio of this two-dimensional model was greater than that of the rotor passages which had a contracting annulus in the final tests.

Photographs of the flow through a model representing the original blading are reproduced in figure 10. Photograph (a) indicates that supersonic flow exists throughout the entire passage. This condition would probably exist in the rotor when the exit pressure is low. Succeeding photographs illustrate the behavior of the normal shock as the model (or the compressor) is throttled.

These photographs indicate that separation occurs in the model passage although much of the observed separation occurs in the corners between the model and the glass walls. Surveys made at the trailing edge of the three-dimensional pressure models indicated similar separation in the models of the same expansion ratio. As previously mentioned, the separation was reduced and total-pressure recovery increased when smaller expansion ratios and larger contraction ratios were employed.

It may be well to explain some of the extraneous effects appearing in the photographs. As the model was so adjusted that the rearward surface of the leading edge was parallel to the entering flow, the entrance wave should be of low intensity and should appear as a single line if the flow is truly two dimensional. In the photographs, the disturbance from the leading edge appears as a wave of considerable width. This effect may be due to a lower velocity of flow along the walls than in the main stream. Some oil is deposited on the glass walls, both inside and out, during the course of a run. This deposit is evident in figure 10, photograph (h), in which some of the lines can be recognized as oil traces. Mach lines ahead of the model are caused by slight irregularities in the nozzle surfaces or are expansion or contraction waves resulting from inequalities between the nozzle exit pressure and atmospheric pressure. As chamber pressures

(total pressures entering nozzle) were automatically controlled to maintain nozzle exit pressure within 0.5 percent of atmospheric pressure, these effects are thought to be small. In general, however, the schlieren photographs are believed to provide a qualitative method of studying the nature of the shock formations.

COMPRESSOR TEST APPARATUS AND METHODS

Test Apparatus

A sectional view of the supersonic-compressor test setup is shown in figure 11 and a photograph of the setup appears in figure 12. Low-turbulence fluid of uniform properties was supplied the annular entrance from the large settling chamber. Three 100-mesh screens were used to reduce the turbulence and swirl. An area reduction of about 30:1 between the cylindrical settling screens and the annular entrance was used to provide uniform flow conditions at the rotor. The diffuser section was lagged to prevent heat leakage between the room air and the test fluid before the shielded diffuser-exit thermocouples were reached. Two water-cooled radiators were used to remove the heat from the circulating fluid. The butterfly throttling valve located in the return section was used to control the exit pressure.

The rotor was driven by a standard aircraft turbosupercharger turbine operated with compressed air, as shown in figure 11. The quantity of compressed air available was sufficient for a running time of only about five minutes. All data for a given point were recorded in this time. The rotational speed was determined from a calibrated electrical tachometer.

In order to reduce structural difficulties and power requirements, the tests were run in Freon-12 at low pressure, usually 0.2 atmosphere. Constant working-fluid composition was maintained by drawing out about 130 cubic feet of the gas per minute, purifying it, and pumping it back into the system. The total volume of the system was about 125 cubic feet. Fluid samples were taken upstream of the settling chamber from the center of the passage. The velocity of sound was measured before and after each run by a sound-velocity meter (reference 3). The composition (usually about 4 percent air) was then determined from a chart prepared from data in reference 4.

Methods

Flow conditions ahead of the test rotor were determined from static pressure measurements taken at various points along the walls of the entrance cone. The static pressure measured at two diametrically opposed points just behind the settling screens was considered to be equivalent to the total pressure, as the velocity of flow was very low ($M \approx 0.026$) at that station. Five thermocouples connected in series were equally spaced around the circumference of the downstream screen to measure the inlet stagnation temperature. The cold junctions of all thermocouples were placed in ice-water baths to provide the same cold-junction temperature at which they were calibrated. The thermocouple potential was read from a calibrated standard-cell potentiometer.

During an early test run, a survey was made of flow conditions behind the guide vanes. A cylindrical yaw tube carrying a total-pressure orifice was used. Measurements were taken every 1/10 inch across the 2-inch annulus along one radial line. End points were taken near each wall. The results of this survey indicated that the desired turning in the entrance vanes (see fig. 2) was produced with only a thin wall boundary layer. The turning angles measured were used in calculations of all runs made with guide vanes. The static pressure ahead of the rotor was measured at points on the inner and outer walls of the inlet annulus. A linear variation of static pressure across the annulus was assumed.

Flow conditions behind the rotor were determined by means of a calibrated survey instrument located approximately 1 inch behind the rotor (figs. 11 and 13) and from orifices located in the walls of the exit annulus. The survey instrument consisted of a "hull" type yawmeter, a static-pressure tube, and a total-pressure tube, shown in figure 14. In tests of the final configuration, measurements were taken at 17 points along one radius (except where otherwise noted). Five shielded thermocouples connected in series were located at equal spaces around the mean diameter of the annular diffuser exit. The exit stagnation temperature, or more usually, the stagnation temperature difference across the compressor, was obtained by measuring the voltage with a calibrated standard-cell potentiometer. Inlet temperatures were controlled to values near room temperature to reduce heat transfer between the test fluid and room air.

All pressure tubes, including a vacuum reference tube, were connected to a mercury manometer. The manometer, thermocouple millivoltmeters, tachometers, and clock were photographed to record the data. The yaw angle behind the rotor and thermocouple potentiometer were read as each photograph was made. Data were

taken with the throttle at various positions at rotational speeds ranging from 5,000 to 12,000 rpm.

Precision of Data

The principal sources of error were in the total-pressure and static-pressure measurements taken in the survey just behind the rotor. Two less likely sources of error were in the static-pressure measurements ahead of the rotor and the angle measurement behind the rotor. Several methods were available for examining these errors. Of these, the most reliable was a comparison of the measured mass flows entering and leaving the rotor. It was thought that the entrance mass-flow measurements were more reliable, and consequently the numerical values for the mass flow were based on the entrance flow.

In the later test runs, which are presented herein, the maximum difference in the mass flows measured at the two stations was 5 percent, with the exception of the run made at 11,500 rpm when the mass flow leaving the rotor was indicated to be 8 percent greater than that entering the rotor. (Survey measurements were taken at only 12 points in this run.) The indicated mass flow leaving the rotor was usually found to be greater than that entering the rotor by an average of 2.1 percent. This difference is to be expected, since total-pressure tubes in turbulent streams tend to read high whereas static orifices may read either low or high, but, in general, the quantity flow measured tends to be too large (reference 5). A check run was made with a standard A.S.M.E. flow-measuring nozzle in the return duct in place of the throttle valve. The mass flow measured through the entrance cone was found to average somewhat lower than that through the nozzle. This result indicates that part of the 2.1 percent average mass-flow error was due to the fact that the entrance reading was low.

In order to evaluate the effects of possible errors on the efficiency and pressure ratio, a test run of average mass-flow error was recomputed in four different ways. In the table which follows, each variable is altered in turn to the extent necessary to balance the mass flow for the average run (average $\Delta G_5 = 2.1$ percent) if no other variable is changed. Actually, the mass-flow discrepancy is most likely to be due to a combination of the more probable errors.

Variable investigated	Increment necessary for mass-flow check (av.)	Effect on $\frac{P_5}{P_0}$	Effect on rotor efficiency, η_r	Effect on thermo-couple efficiency, η_{ad}
P_5	4.5 percent	No change	4.5 percent	Negligible
P_5	-1.1 percent	-1.1 percent	-1.1 percent	-2 percent
θ_5	1.5°	No change	-2.0 percent	Negligible
P_1	-2.7 percent	No change	-.13 percent	No change

During a few of the final runs, the stagnation temperature difference across the compressor was measured with a potentiometer. From these values, compressor efficiencies based on the survey total pressure were obtained. These temperature-rise efficiencies η_{ad} averaged about 1.1 percent lower than the efficiencies obtained from the survey measurements but showed appreciable scatter and are therefore not presented.

Construction of Rotor

The first rotor tested had no shroud and was constructed with Swedish spring steel blades. These blades were given the desired curvature at the root by means of formed dural holding pieces inserted into slots in the rim and were held in with shear pins extending through the holding pieces and the blades. (See fig. 15.) Centrifugal loads were to extend the curvature to the outer blade regions when the compressor was operated. However, these Swedish steel blades - having little internal damping and low vibrational frequencies - failed after a very short running time as a result of vibrational stresses.

In order to eliminate these vibration difficulties, it was thought necessary to increase the natural frequencies by restraining the blades with a shroud attached to the tips. As a safeguard against difficulties resulting from high-frequency vibration, annealed 18:8 chromium-nickel steel was used in making the blades and shroud sections. The blade tips were inserted in curved slots in the shroud and silver soldered in place (fig. 16). Connecting the shroud sections accurately, however, proved very difficult and considerable variation of blade angle and spacing resulted at the shroud joints. In addition, warping occurred during the silver-soldering operations, both in repairs that subsequently were made,

as well as in the original assembly. A maximum variation in the spacing of the blades of about 25 percent was measured at the tips where the discrepancies were the largest. Because of the warpage in the shroud, all the blades buckled slightly so that the pitch sections were straight instead of being curved 8.8° as intended. The angle between the blade chord line and the axis, the contraction ratio, the turning of the passage between the blades, and the expansion ratio of the compressor blades varied from blade to blade. Only rough average values of these important factors could be obtained, and only nominal values of the expansion and contraction ratios are presented for purposes of comparison. The important inaccuracies in the construction of this rotor mean that the test results have only qualitative significance. The rotor has been rebladed more accurately and is being tested.

The supersonic compressor was first run in air at atmospheric pressure to test the operation of the mechanical design. It was found that the shroud moved downstream with a displacement increasing with the rotor speed. At a rotor speed of 11,000 rpm, which was about the maximum used in Freon-12, the shroud moved about 0.050 inch from its static position. Whether this displacement was accompanied by twisting of the outer portion of the blades has not been determined, but the possibility does exist. The motion of the shroud, in addition to its poor construction, made difficult the sealing of the gap between stationary and rotating parts. A strip overlapping the leading edge of the shroud was attached to the outer casing just ahead of the rotor. (See fig. 1.) At best, considerable leakage must have occurred through the gaps ahead of and behind the shroud.

RESULTS OF COMPRESSOR TESTS

Early Test Runs

Aerodynamic data were first taken of the experimental supersonic compressor on May 24, 1945. The rotor was tested in its original condition, with the outward curvature of the shroud. Very low pressure rises and efficiencies were obtained. No performance discontinuities were observed in accelerating the compressor to a Mach number of 1.5. A survey behind the rotor indicated low total pressure and high turning angle at the outer portion of the blades. Because of the separation at the tip, little diffusion occurred within the blade passages and high exit velocities resulted at the smaller diameters. The contraction ratio was 1.035. Results of total-pressure and turning-angle surveys for runs 12 through 18, excluding run 15, are shown in figure 17.

All these runs were made at a rotational speed of 10,000 rpm at maximum pressure rise.

In run 12 (fig. 17), balsa was added to the shroud underside so that the underside was cylindrical in shape and the expansion ratio was reduced to $E_R = 1.223$. This first alteration led to increased pressure ratio as well as to better total-pressure distribution, although the flow at the tip was still very badly separated. The previously observed condition of lower total pressure at the tip than at the root was still evident. Also, the angle of flow at the tip indicated a large separated region. The efficiency obtained was about 50 percent, the survey pressure ratio was 1.52, but the mass-flow discrepancy was quite large. In run 13, the chamber pressure was raised from the previously used 1/10 atmosphere to 2/10 atmosphere in order to improve the purity of Freon-12 and the precision of measurement. As shown in figure 17, values for run 13 are little changed from those for run 12. The accuracy of the readings at higher pressures appeared to be improved.

The next important change was thickening the rotor blades toward the trailing edges with balsa wood on the blade sides to reduce the expansion following the minimum section to a value of $E_R = 1.091$. Tests of the compressor with this alteration were made in run 14. This reduced expansion resulted in higher measured pressure ratios, little change in total-pressure distribution, and a desirable reduction in the flow angle at the tip. (See fig 17.) A pressure ratio of 1.56 was obtained with an efficiency of 70 percent from survey measurements.

The fact that no discontinuity existed in the transonic range seemed to indicate that the contraction ratio could be increased advantageously. It was therefore decided to increase the contraction ratio from 1.035 to approximately 1.15 in run 15. Balsa wood was glued to the rotor blades to give the larger contraction ratio. In this condition, flow entering the rotor did not approach the supersonic operating condition, inasmuch as the maximum axial velocities and mass flow measured were very low. Little pressure rise was observed. The contraction ratio of 1.15 was apparently too large for the maximum blade entrance Mach number obtainable with the existing equipment. The original contraction ratio of 1.035 was therefore used in two subsequent runs.

The results of run 14 had indicated that the reduced expansion caused some improvement in performance. The thick trailing edges were undesirable, however, and thus, it was decided to maintain the expansion ratio of run 14 by reducing the annular passage height and removing the balsa from the sides of the blades. This modification was tested in run 16. Figure 17 shows good distribution

of the total pressure and turning angles for run 16. A survey pressure ratio of 1.72 was measured with an efficiency of 79 percent.

Run 17, in which 1/16 inch of balsa was removed from the underside of the shroud at the exit to increase the expansion ratio to 1.135, failed to show significant improvement in performance over run 16, yielding a measured pressure ratio of 1.66 at an efficiency of 81 percent. The distribution of the yaw angles and total pressure was not so good as in the previous run. It now seemed that the optimum expansion ratio had been determined, but the pressure ratio desired could not be obtained with the small amount of subsonic diffusion apparently obtainable with this blading. Again, increased contraction ratio appeared to offer the most promising method of improving performance.

The expansion ratio of the rotor for run 18 was the same as that for run 16, $E_R = 1.091$, but the contraction ratio was increased to 1.092 (fig. 6) by gluing balsa wedges to the sides of the blades. The performance was considerably improved, but the distribution and yaw angles were not. With the exception of improved balsa surfaces, the rotor remained as in run 18 throughout the rest of the test period. Theoretical velocity diagrams were developed for this configuration for air (fig. 2(b)) and for Freon-12 (fig. 2(c)).

The compressor showed the same general trends as the static models. Improved operation was obtained with increased contraction ratio, and best performance occurred at expansion ratios of about 1.1. The diffusion in the rotor, however, was much less efficient and the exit velocity was very high (fig. 18(c)). This result was due probably, in part, to the inaccurate construction of the rotor. As previously mentioned, the rotor has been rebladed more accurately; this investigation is being repeated and extended in an attempt to obtain improved performance.

Tests of Final Rotor Configuration

The final configuration of the rotor was tested in Freon-12 at 0.2 atmosphere from a compressor Mach number $M_c = 0.7$ to $M_c = 1.6$, corresponding to rotational speeds from 11,000 rpm to 25,000 rpm in air at static sea-level conditions. Most of the runs were made with the guide vanes, but a few crude tests were made without the guide vanes. (See appendix C.) A straight annular passage was used behind the rotor (solid lines, fig. 1). The Reynolds number (see appendix D) at the design conditions in Freon-12, about 650,000, was about half the value that would result in air at static sea-level entry conditions.

Conditions behind the rotor were determined by surveys taken just downstream from the rotor. Results of typical surveys from tests run with and without guide vanes are presented in figure 18. The performance of the compressor as obtained from such surveys is presented in figures 19, 20, 21, and 22. The rotor efficiency showed little change with rotational speed, varying from 82 percent at $M_c = 0.7$ to 83 percent at $M_c = 1.3$, and to 80 percent at $M_c = 1.5$. The measured pressure ratio showed a linear increase with compressor Mach number in the higher speed range, reaching a maximum value of 1.96 at a compressor Mach number $M_c = 1.57$. Velocity diagrams obtained from measurements at the design speed (10,500 rpm) are presented in figure 2(d). Figures 19 and 20 show that the experimental compressor produced a pressure ratio of 1.8... with a rotor efficiency of 0.83 and a mass-flow coefficient C_G of 0.395, which when converted to static sea-level atmospheric conditions is equivalent to 28.5 pounds of air per second. If it were possible to install stator blades capable of recovering 90 percent of the dynamic pressure, the over-all efficiency would be about 80 percent. The high mass flow and pressure ratio make this compressor more compact by a factor of about 4 than any other known machine performing the same operation.

DISCUSSION

Supersonic Operating Condition

Large total-pressure losses occur in extended strong shock waves. These losses can be largely prevented if the strong shocks are confined within properly designed blade passages. In reference 2, it was shown that this effect cannot be obtained with finite blade thickness at Mach numbers close to 1. As an aid to understanding the flow patterns at these transonic Mach numbers, a hypothesis proposing that detached bow waves were formed ahead of each blade was presented. Speeds above the minimum at which detached bow waves could be expected to attach themselves to the blading are classified as the supersonic operating condition. One of the first objects of this work was to determine whether such a supersonic operating condition could be found with the test compressor; that is, whether a regime of operation existed which agreed with the theoretical considerations for the supersonic operating condition discussed in reference 2.

One of the first inferences from this theory would be that the volume flow entering the compressor could be determined by the requirement that the entering air direction be parallel to

the rearward side of the blades at the leading edge (this portion of the blades was essentially flat in this compressor). In figure 22, it can be seen that for entering Mach numbers M_{2p} greater than about 1.43, the rotor entrance angle is apparently independent of rotational speed and of throttle position. The actual angle measured in this range is of the order of 28° which is to be compared with the 30° called for in the design. This agreement is considered good in view of the numerous structural inaccuracies of this compressor.

It would also be expected that, in the supersonic operating range, the losses would be primarily due to the shock waves and resultant separation occurring inside the rotor passages. Experience with supersonic diffusers (reference 1) has indicated that these losses decrease as the exit pressure on the passages is increased. It would be expected, therefore, that highest efficiency would be obtained with maximum exit pressure; that is, at maximum pressure ratios. Some evidence that this effect was obtained can be found from the efficiencies of the highest speed runs (10,500 rpm) in figure 20.

Furthermore, the lowest Mach number at which these supersonic operating characteristics would appear (starting Mach number) should be related to the contraction ratio of the blade passages in a manner similar to the starting curve (fig. 3 of reference 1) for supersonic diffusers. Since the contraction ratio in this blading was about 1.092, it would be expected that the supersonic operating condition in Freon-12 would occur for Mach numbers M_{2p} of about 1.43 or greater, or for compressor Mach numbers (compare with fig. 22) of 1.34 or greater. The characteristics of the supersonic operating condition, which were referred to previously, apparently begin at Mach numbers very close to these values. The expected drop in efficiency due to increased shock losses at higher Mach numbers than design was found, as is evident in figures 20 and 21.

Transonic Operating Condition

In the transonic range, detached bow waves would be expected to exist ahead of the leading edges of the rotor blades. These waves should have two kinds of effects on the performance of the compressor. In the first place, the rotor entrance angle would be reduced below the value which is found in the supersonic operating condition, as is indicated in reference 2. The

experimental values are given in figure 22, and it can be seen that the reduction of this angle at low Mach numbers did occur. This effect can also be seen in the mass-flow curves of figure 19. Furthermore, the amount of the reduction is seen to depend greatly on the exit pressure. The results obtained at 9000 rpm are particularly interesting in this respect. It can be seen that the exit pressure could be increased up to a certain point without having any effect on the mass flow. Thus, it seems likely that up to this point, the flow through the blade passages was, at least in part, supersonic so that the exit pressure had no effect on the detached bow-wave system. Higher exit pressures apparently resulted in a subsonic flow through the blade passages and in this range, the mass flow and hence, also, the strength of the detached bow-wave system was affected by the exit pressure.

The second effect to be expected from the detached bow-wave system is that the losses inherent in this system should appear in the measured efficiencies. These losses can be seen in two ways in the experimental results. First, it will be seen that the peak efficiency did not begin to drop off with Mach number until the supersonic operating condition was reached (fig. 21). It is well known that the efficiency of supersonic diffusion decreases, in general, with increasing Mach number. Thus, it seems reasonable to conclude that in the transonic range, the expected drop in efficiency is compensated - or apparently slightly overcompensated - by the bow waves coming closer to attachment and thus the loss in the bow-wave system is decreased. Second, it can be noticed in figure 20 that the peak efficiency does not occur at peak pressure ratio in the transonic range. Some indication can be seen in this figure that peak efficiency tends to move closer to peak pressure ratio as the supersonic operating condition is approached. The transonic performance also shows a distinct departure from the performance of supersonic diffusers, since in supersonic diffusers, peak pressure ratio and peak efficiency always occur simultaneously. It is considered that the drop in efficiency for higher pressure ratios at a given Mach number is due to an increase in the strength and in the losses of the detached bow-wave system.

In these experiments, no discontinuity of any kind was observed in the flow as the compressor passed through the transonic range. This performance was considered somewhat surprising in view of the fact that most supersonic diffusers show discontinuous performance when the shock wave is swallowed. The reasons for this lack of discontinuity are not yet clearly understood and, therefore, no prediction as to whether discontinuities will be found in other supersonic compressors can be made. There is a

possibility that this lack of discontinuity is related to the high level of disturbances which must be present due to the separation in the rear of the rotor passages, which will be discussed. This subject needs further study.

Some understanding of this performance can be had, however, on the basis of the detached bow-wave hypothesis. As the relative Mach number is increased, the bow waves would be expected to approach attachment. At the instant of attachment, the downstream leg of the bow wave, which now forms a normal shock in the passage (fig. 4, reference 2) would probably jump downstream to a stable position in the diverging part of the rotor passage. Since the mass flow and throttle position are unchanged by this sudden motion of the shock wave, the back pressure on the compressor would also be expected to be unchanged. Therefore, it would seem that, in accelerating a compressor, attachment of the bow waves would produce no sudden effect in the observed performance.

Experimental Results on the Flow Leaving the Rotor

From the previous discussion, the supersonic flow entering the rotor appears to be fairly well understood qualitatively. The situation in regard to the flow leaving the rotor is not nearly so well understood. A marked discrepancy was found between the efficiency of diffusion in the 1-inch-jet tests and in the rotating machine. Thus, in the 1-inch-jet tests, it was possible to diffuse to Mach numbers of the order of 0.6; whereas, in the rotor, exit Mach numbers (fig. 18(c)) of about 0.95 were measured. It is apparent also that a large part of the slowly moving air in the rotor passage appeared at the tip section. In test runs 12 and 13, where the expansion ratio of the subsonic passage was large, this effect was very greatly accentuated.

The high total-pressure losses, and particularly the accumulation of slow air at the tip, produce serious discrepancies between predicted and experimental performance. In the first place, the pressure ratio obtained by the compressor was very greatly reduced from the design value of about 2.9 to about 1.8. This great difference in pressure ratio can be best explained by considering several factors in combination. First, the Mach number leaving the rotor was higher and thus produced a lower static pressure in addition to the static pressure drop attributable to the increased total-pressure loss. Higher velocities leaving the rotor (rotor coordinates) meant also lower velocities entering the stator (stator coordinates), and consequently, lower total pressure measured entering the stator (fig. 2). The pressure ratio obtained in the

supersonic compressor therefore appears to be very sensitive to the diffusion efficiency in the rotor passages. The measured efficiency, about 80 percent, was lower than the predicted value calculated from the results of the 1-inch-jet tests, which was about 90 percent. These values, however, still do not take into account the difficult problem of the stator design occasioned by the fact that the velocity and total pressure of the air behind the rotor tip would be considerably lower than that behind the pitch or the root and would be accompanied by the appreciable variation in flow direction measured across the exit annulus.

Velocity diagrams from data taken in actual tests at design speed in Freon-12 are presented in figure 2(d). It is to be noted that the tip section shows turning in a direction opposite to that of the blade camber whereas the pitch section shows too large a turning in the expected direction. These effects are probably due to the radial flows necessitated by separation at the tip.

The reasons for the increased loss in the rotating tests are not yet clear. Three effects which existed in this compressor should be pointed out. First, the construction of this machine is particularly defective at the blade tips, and these construction defects undoubtedly increased tip losses. Second, the presence of the shroud and resultant leakage probably affect the flow adversely. Third, the interaction of a normal shock with the boundary layer usually results in a great thickening of the boundary layer. It would be expected that these thick boundary layers would be centrifuged toward the tip of the rotor and thicker dead-air regions would thus be created at the tip than at the root.

One preliminary attempt that was made to reduce the accumulation of slow air at the tip should be mentioned. In the original design, the entrance vanes roughly equalized the total pressure entering the tip with that entering the root of the rotor. If these entrance vanes were removed, the total pressure relative to the rotating blades entering the tip would be expected to be higher than that entering the root. These vanes were therefore removed in the hope that the increased total pressure entering the tip might help to remove the accumulation of slow air at this point. The results obtained can be seen in figure 18 and appendix C. From these results, it is apparent that some improvement in the flow leaving the rotor was made in this way. The efficiencies calculated from these runs were somewhat higher than those obtained previously, but these results are not presented since the measured mass flows entering and leaving the rotor did not check and these experiments must be repeated. Procedures of this general nature are considered, however, to have great promise.

The study of this problem was made very difficult because of the construction defects of the present rotor and further research on a reconstructed rotor is in progress.

PRELIMINARY TESTS OF REBLADED ROTOR

A few preliminary tests have been run with an accurately rebladed rotor to provide a rough evaluation of the effects of inaccurate construction on the performance of the previous rotor. Although the contraction ratio of the blades in the new rotor is low, about 1.035, the expansion ratio has the value found to be optimum in the old rotor $E_P = 1.091$. Test results are encouraging. Flow conditions across the exit annulus have been found to be quite uniform and higher survey efficiencies have been obtained with some increase in pressure ratio. These more uniform flow conditions should make possible the design of an efficient stator to follow the rotor. A stator is being installed and will be tested.

CONCLUDING REMARKS

An experimental single-stage supersonic axial-flow compressor has been designed, built, and tested in Freon-12. This 16-inch-diameter compressor produced a pressure ratio of 1.8 with a rotor efficiency of 83 percent and a mass flow (converted to sea-level static atmospheric conditions) equivalent to 28.5 pounds of air per second. If a 90 percent dynamic-pressure recovery is assumed to be attained through the stator (it is not at all clear that an efficient stator could be added to the rotor tested), the over-all efficiency would be about 80 percent.

In the supersonic operating condition, the mass flow is independent of the pressure ratio. This performance is also typical of high-performance multistage subsonic axial-flow compressors. Peak efficiency was obtained at maximum pressure ratio. These characteristics, as well as the quantitative mass flow measured, are in agreement with theoretical considerations. This agreement should justify the general application of theoretical supersonic gas dynamics to the design of these machines.

In the transonic range, the operation and performance showed no discontinuity in passing from the subsonic to the supersonic operating condition. The peak efficiency occurred at less than the maximum pressure ratio with values only slightly below the

supersonic efficiency peaks. Mass-flow variation with pressure ratio (at a given rotational speed) decreased as the supersonic operating condition was approached. These characteristics can be explained by the detached bow-wave hypothesis.

The diffusion process in the rotor passages was found to be much less efficient than the diffusion in simulated rotor passages in the stationary tests. The pressure ratio produced by a compressor of this type is very sensitive to the efficiency of diffusion in the rotor passages, and this low efficiency caused a large drop from the design pressure ratio. Much of the low-energy air accumulated at the tip of the rotor and the resultant poor distribution in angles and total pressure would make difficult the design of an efficient stator to follow this rotor. There are, however, several approaches available for improving the efficiency of diffusion in the rotor passages and equalizing the root and tip efficiencies. The study of this problem was made very difficult because of the construction defects of the rotor tested and further research on a reconstructed rotor is in progress.

Compressors having supersonic velocities relative to the blading show considerable promise for application to aircraft propulsion engines. With only slight improvements in performance, the supersonic compressor will be able to compete with existing compressors, particularly in turbojet engines where compactness and light weight are essential. It should then be possible to design a machine which would be about four times as compact as any other known compressor performing the same operation.

Langley Memorial Aeronautical Laboratory
National Advisory Committee for Aeronautics
Langley Field, Va.

APPENDIX A

TOTAL-PRESSURE RECOVERY BY STATIC-PRESSURE MEASUREMENTS

When the flow conditions at the exit cross section of a supersonic diffuser are uniform, it is possible to calculate accurately the recovered total pressure by use of the expression obtained in the following derivation:

From the energy equation

$$c_p T_{2s} = c_p T_2 + \frac{V_2^2}{2}$$

and

$$c_p T_{4s} = c_p T_4 + \frac{V_4^2}{2}$$

then

$$V_2 = \sqrt{2c_p (T_{2s} - T_2)}$$

and

$$V_4 = \sqrt{2c_p (T_{4s} - T_4)}$$

From the equation of state

$$\rho_2 = \frac{P_2}{RT_2}$$

and

$$\rho_4 = \frac{P_4}{RT_4}$$

From considerations of continuity

$$\rho_2 V_2 A_2 = \rho_4 V_4 A_4 \quad (1)$$

Substituting in equation (1) gives

$$\frac{P_2}{RT_2} A_2 \sqrt{2c_p (T_{2s} - T_2)} = \frac{P_4}{RT_4} A_4 \sqrt{2c_p (T_{4s} - T_4)} \quad (2)$$

Squaring both sides, canceling common factors, and transposing leads to

$$\left(\frac{P_2}{P_4} \frac{T_4}{T_2} \frac{A_2}{A_4} \right)^2 (T_{2s} - T_2) = T_{4s} - T_4 \quad (3)$$

From equation (3), if it is assumed that $T_{2s} = T_{4s}$, and use is made of the quadratic formula, the adiabatic relationship between the stream and stagnation conditions at the blade exit being included, the following expression is derived from which P_4 may be calculated:

$$\frac{P_4}{P_2} = \frac{\left[1 + \sqrt{1 + 4 \left(\frac{P_2}{P_4} \frac{A_2}{A_4} \right)^2 \left(\frac{T_{2s}}{T_2} \right) \left(\frac{T_{2s}}{T_2} - 1 \right)} \right]^{c_p/R}}{2} \quad (4)$$

APPENDIX B

PERFORMANCE COMPUTATION METHODS

Mass flow.- The entrance mass flow is computed from the measured data, R , p_0 , p_1 , T_{1s} , and θ_1 for each radial survey station r between the root and tip of the rotor inlet annulus. The exit mass flow is computed from the measured data p_5 , P_5 , T_{5s} , and θ_5 over the exit annulus. The expression for inlet mass flow $G_1 = \rho_1 V_1 A_1$ may be written in the differential form $dG_1 = \rho_1 V_1 dA_1$. In the final form the expression becomes

$$G_1 = \int_{r_h}^{r_t} 2\pi \frac{p_1}{RT_1} V_1 \cos \theta_1 r_1 dr_1$$

the right side of which may be integrated mechanically when plotted against the inlet-annulus radii. The analogous expression

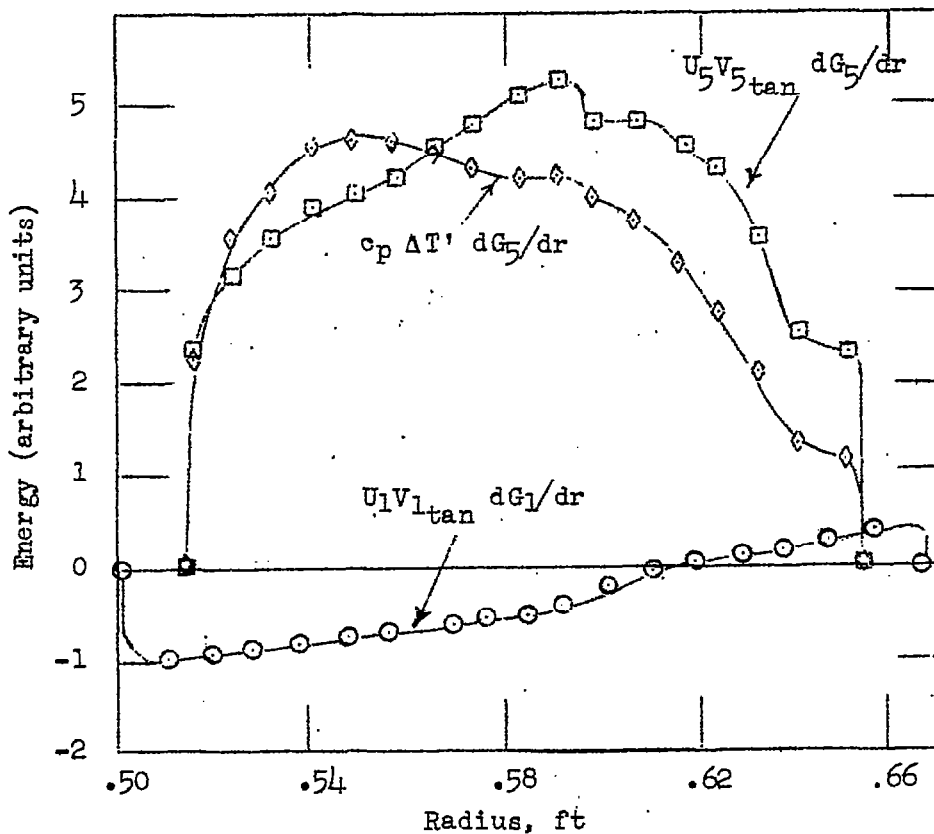
$$G_5 = \int_{r_h}^{r_t} 2\pi \frac{p_5}{RT_5} V_5 \cos \theta_5 r_5 dr_5$$

may be similarly integrated to give the exit mass flow as a check of the precision of measurement. The mass-flow coefficients C_G are found by dividing the computed mass flow by $\left(\frac{2}{\gamma+1}\right)^{\frac{\gamma+1}{2\gamma-2}} \rho_0 a_0 A_{disc}$ or $\rho_{cr} a_{cr} A_{disc}$ which is the maximum possible mass flow through a disc having the same tip diameter.

Efficiency.- The rotor efficiency η_r is computed from the following expression (the velocity vectors are shown in fig. 2):

$$\eta_r = \frac{G c_p \Delta T'}{G U \Delta V_{tan}} = \frac{\int_{r_h}^{r_t} c_p \Delta T' dG_5}{\int_{r_h}^{r_t} U_5 V_{5tan} dG_5 - \int_{r_h}^{r_t} U_1 V_{1tan} dG_1}$$

Typical plots of the terms of this expression are shown in the following figure. The efficiency may be obtained by integration of these plots.



Weighted average pressure ratio.- The pressure ratio is measured at each survey station directly behind the rotor. The weighted average pressure ratio is found from the following relations:

$$\Delta T'_{wt} = \frac{\int_{r_h}^{r_t} \Delta T' dG_5}{G_5}$$

$$\left(\frac{P_5}{P_0}\right)_{wt} = \left(1 + \frac{\Delta T'_{wt}}{T_0}\right)^{c_p/R}$$

APPENDIX C

TEST RESULTS WITHOUT GUIDE VANES

The over-all performance of the compressor was improved by the removal of the guide vanes; however, the magnitude of improvement was not great enough to warrant a complete series of new tests with the same inaccurately constructed rotor. The results of those tests run without vanes are listed as follows:

Rotational speed (rpm)	M_c	$\frac{P_2}{P_1}$	η_r	Mass-flow discrepancies (percent)
9,000	1.243	1.582	80.48	2.8
10,000	1.331	1.709	86.85	8.8
10,000	1.351	1.727	81.96	6.0
10,500	1.414	1.808	88.00	13.0
10,500	1.434	1.826	83.00	7.3
11,000	1.498	1.900	81.80	7.6
11,500	1.576	1.970	78.90	7.9

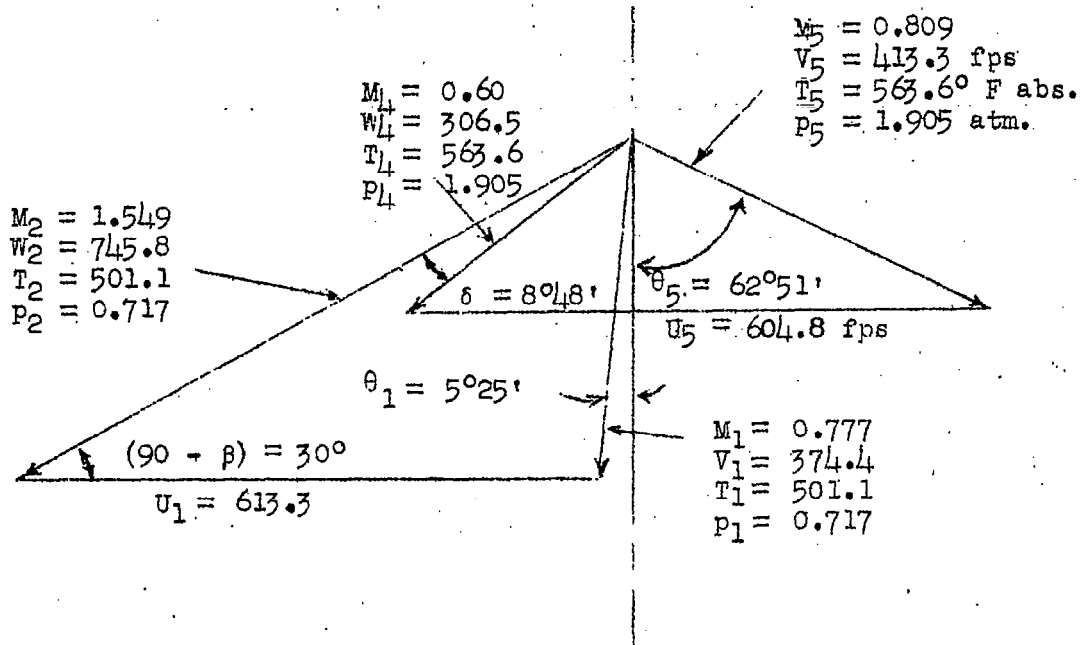
The discrepancies between the mass flow entering the rotor and that leaving the rotor were quite large for these vaneless runs. These data were therefore considered inaccurate, some of the efficiencies in particular appearing too high.

APPENDIX D

COMPARISON OF FREON-12 AND AIR AS TESTING MEDIA

In order to make aerodynamic tests at lowered tip speeds with reduced stresses in the rotor, but at design Mach numbers, Freon-12 was used as the testing medium because of its low velocity of sound, about half that of air. Like air, Freon-12 ($\text{C Cl}_2 \text{ F}_2$) behaves very nearly as a perfect gas at room temperatures and pressures, approaching this behavior even more closely at the lower pressures used in these tests (reference 4). This gas, however, has physical properties somewhat different from air, with a value of $\gamma = 1.125$ at 0.2 atmosphere, 580°F absolute as compared with $\gamma = 1.4$ for air at standard conditions. Although the adiabatic flow relationships of pressure and mass flow per unit area with Mach number are about the same in Freon-12 and in air in the range considered, the temperature, contraction-ratio, and shock-loss relations with Mach number are significantly different. The temperature change in Freon-12 is about a third that in air for a given adiabatic pressure change. For example, the permissible contraction ratio for Freon-12 is about 1.12 compared to 1.09 for air at a Mach number of 1.50 relative to the blades. Total-pressure losses in shock waves are somewhat greater in Freon-12 than in air for a given pressure ratio or a given Mach number. Reynolds numbers for the design condition, based on a blade chord length of 0.1355 feet and typical flow conditions entering the rotor (fig. 2) are about 650,000 in Freon-12 compared to about 1,100,000 in air.

Because of these various differences, aerodynamic tests conducted in Freon-12 would produce somewhat different results than if they were conducted in air; particularly when a change in physical coordinate system is involved, as in compressors. The following velocity diagram is given to compare the flow conditions which would occur at the pitch section when the compressor is run at the same compressor Mach number, $M_c = 1.43$, in Freon-12 as in air. These values are to be compared with the velocity diagrams for the pitch section (fig. 2(a)).



From this example, it is obvious that the Mach number entering the blades is considerably lower in Freon-12 ($M_2 = 1.54$) than in air ($M_2 = 1.62$). Inasmuch as M_2 is probably the most important parameter that determines the operation of the compressor, comparisons should be made on this basis, rather than on the basis of M_c . In figure 2, velocity diagrams for air (fig. 2(b)) and for Freon-12 (fig. 2(c)) present the flow conditions with the same Mach numbers entering the blades.

Some differences in the flow conditions are evident. The total pressure, Mach number, and flow angle entering the stators are higher in Freon-12. The calculated efficiencies are about the same in either case, 86 percent if normal shock losses and 90 percent dynamic-pressure recovery in the stator are assumed.

It is clear from the foregoing discussion that, if a compressor is to be tested in Freon-12, the aerodynamic design calculations must be based on the flow relationships for Freon-12 if the results are to be more than roughly qualitative. If such results are used

to design an air compressor, care must be exercised because the flow conditions will not be identical. However, as these corrections can be made, Freon-12 does provide a testing medium for exploratory investigations in which it is desirable to reduce the structural problems and power requirements.

REFERENCES

1. Kantrowitz, Arthur, and Donaldson, Coleman duP.: Preliminary Investigation of Supersonic Diffusers. NACA ACR No. L5D20, 1945.
2. Kantrowitz, Arthur: The Supersonic Axial-Flow Compressor. NACA ACR No. L6D02, 1946.
3. Huber, Paul W., and Kantrowitz, Arthur: A Device for Measuring Sonic Velocity and Compressor Mach Number. NACA RM No. L6K14, 1947.
4. Huber, Paul W.: Use of Freon-12 as a Fluid for Aerodynamic Testing. NACA TN No. 1024, 1946.
5. Nielsen, Jack N.: Effect of Turbulence on Air-Flow Measurements behind Orifice Plates. NACA ARR No. 3G30, 1943.

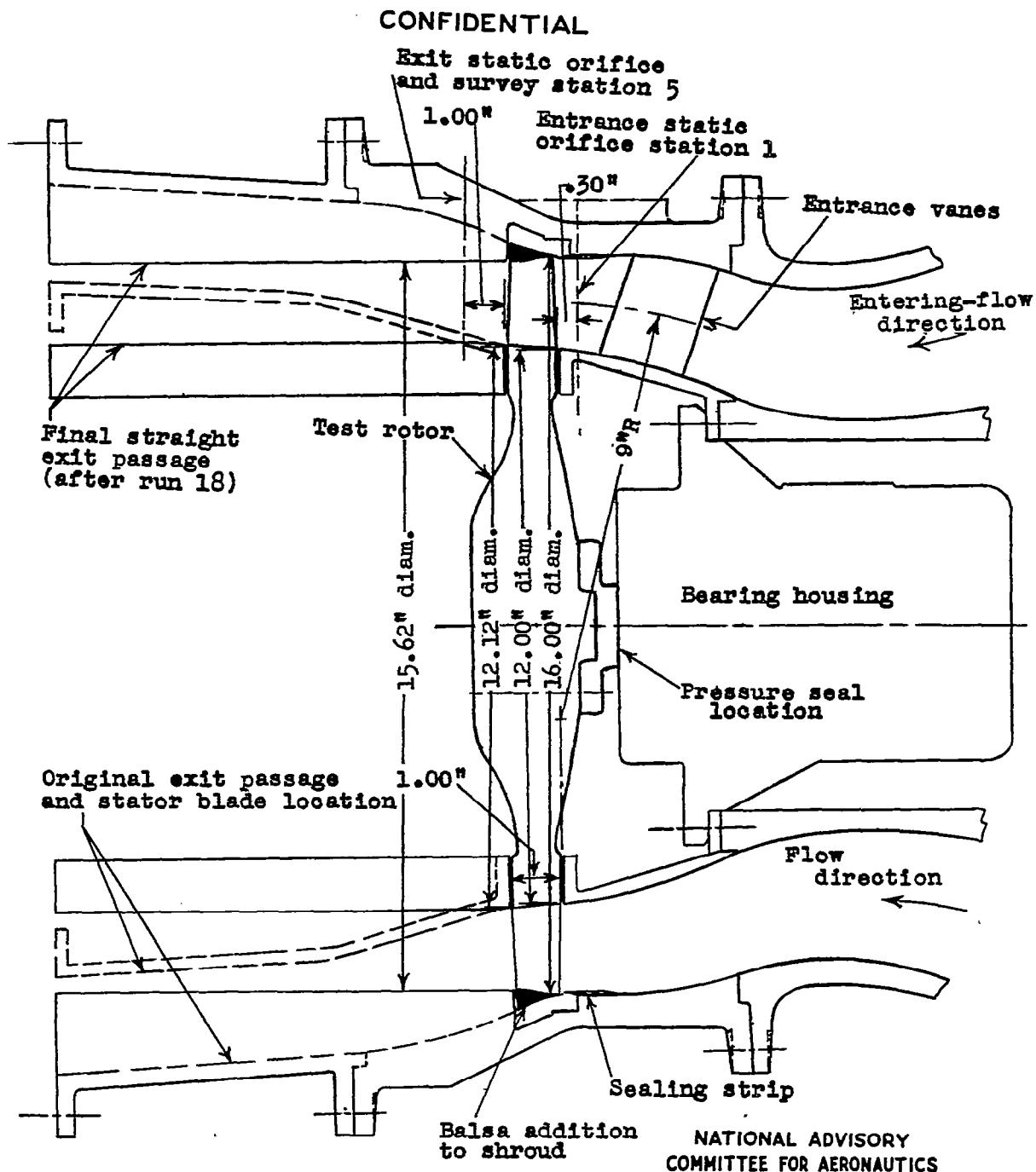
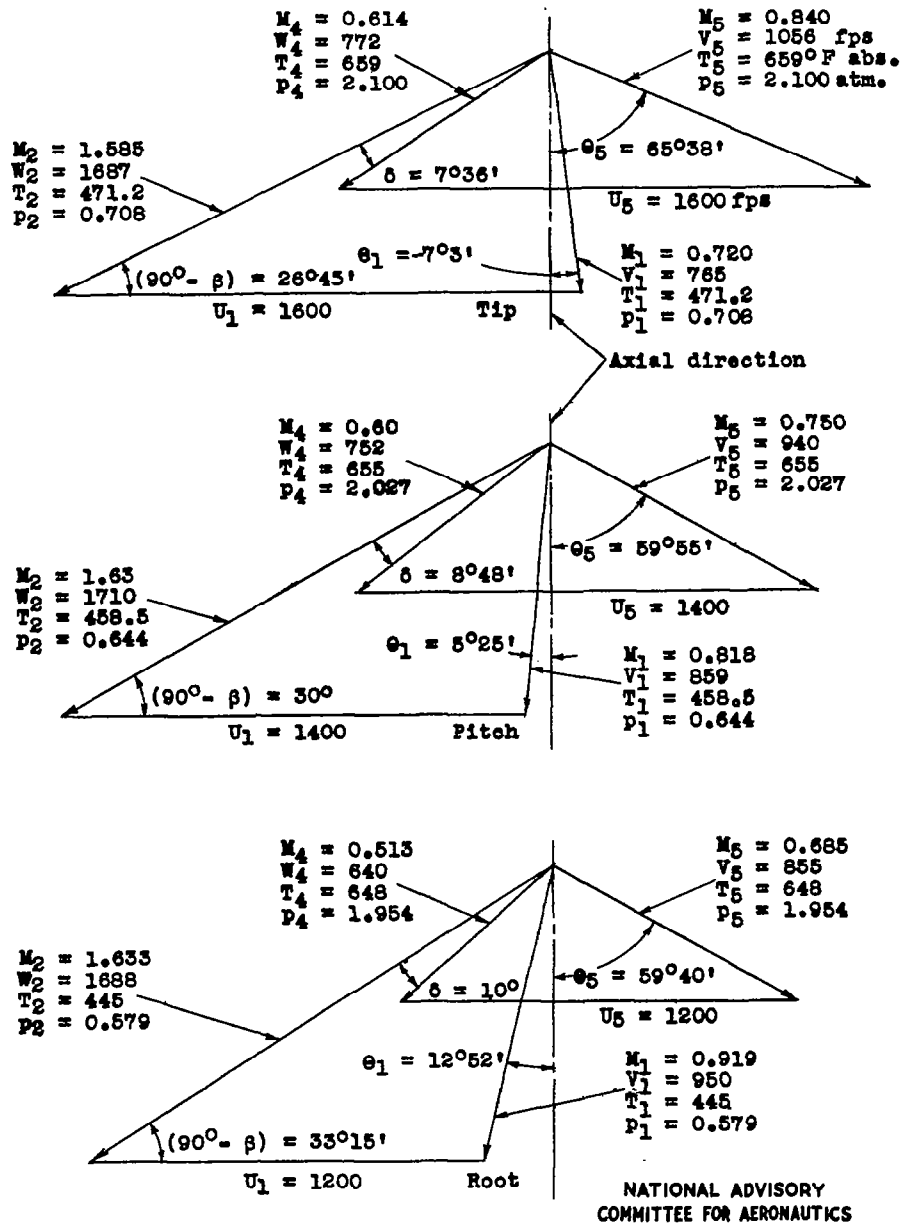


Figure 1.- Longitudinal section through the rotor showing aerodynamic passages. The original outward curvature of the shroud and exit passage are shown as dashed lines.

CONFIDENTIAL

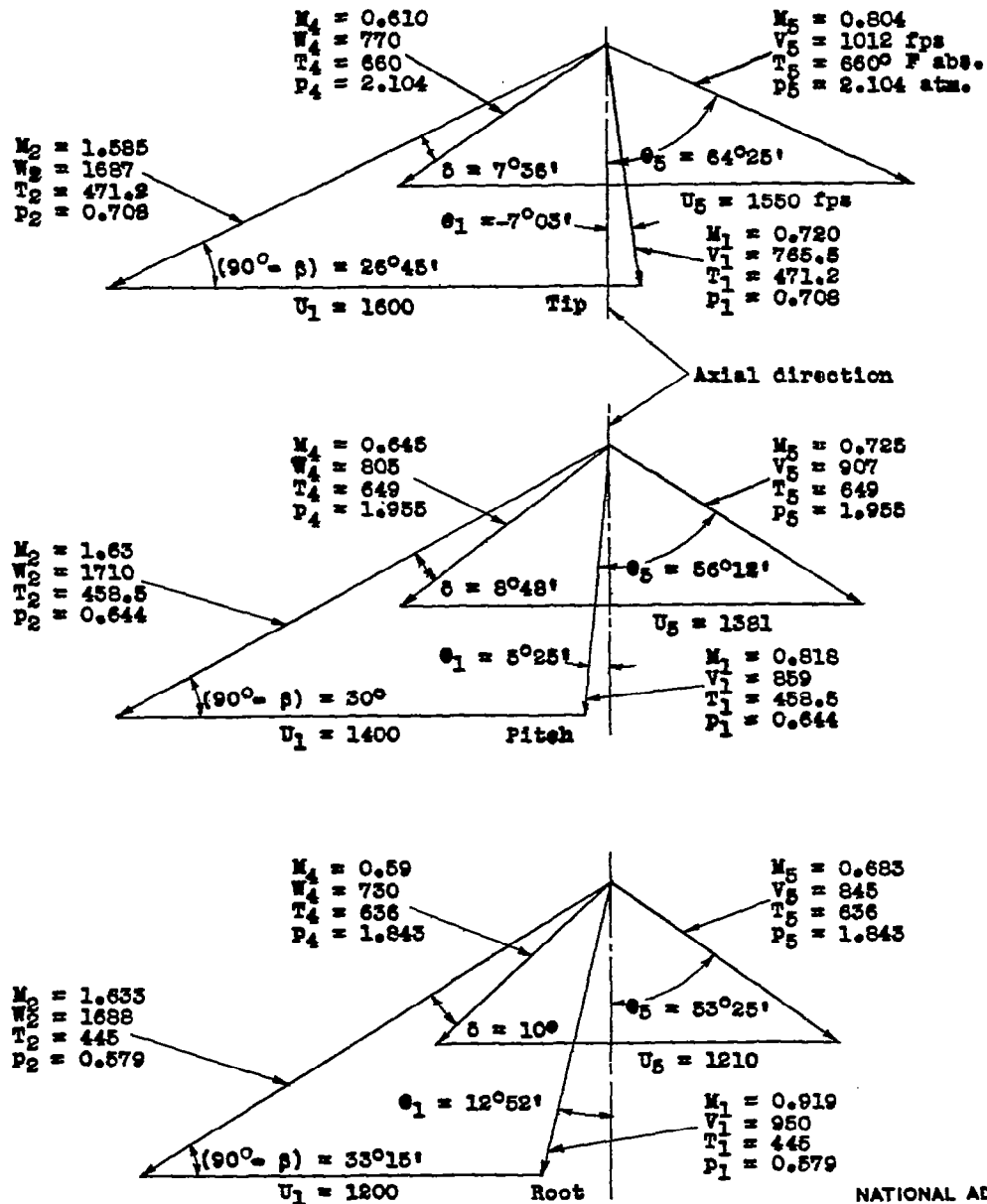


(a) Original velocity diagrams for air, based on rough preliminary 1-inch-jet tests. Initial conditions: $p_0 = 1.00$ atmosphere; $T_0 = 520^\circ\text{F absolute}$. Final weighted stagnation conditions: $T_{5s} = 730.1$; $\frac{P_5}{P_0} = 2.99$; and, with stator losses neglected, $\eta_r = 90.9$ percent.

Figure 2.- Supersonic-compressor velocity diagrams for the tip, pitch, and root sections.

CONFIDENTIAL

CONFIDENTIAL

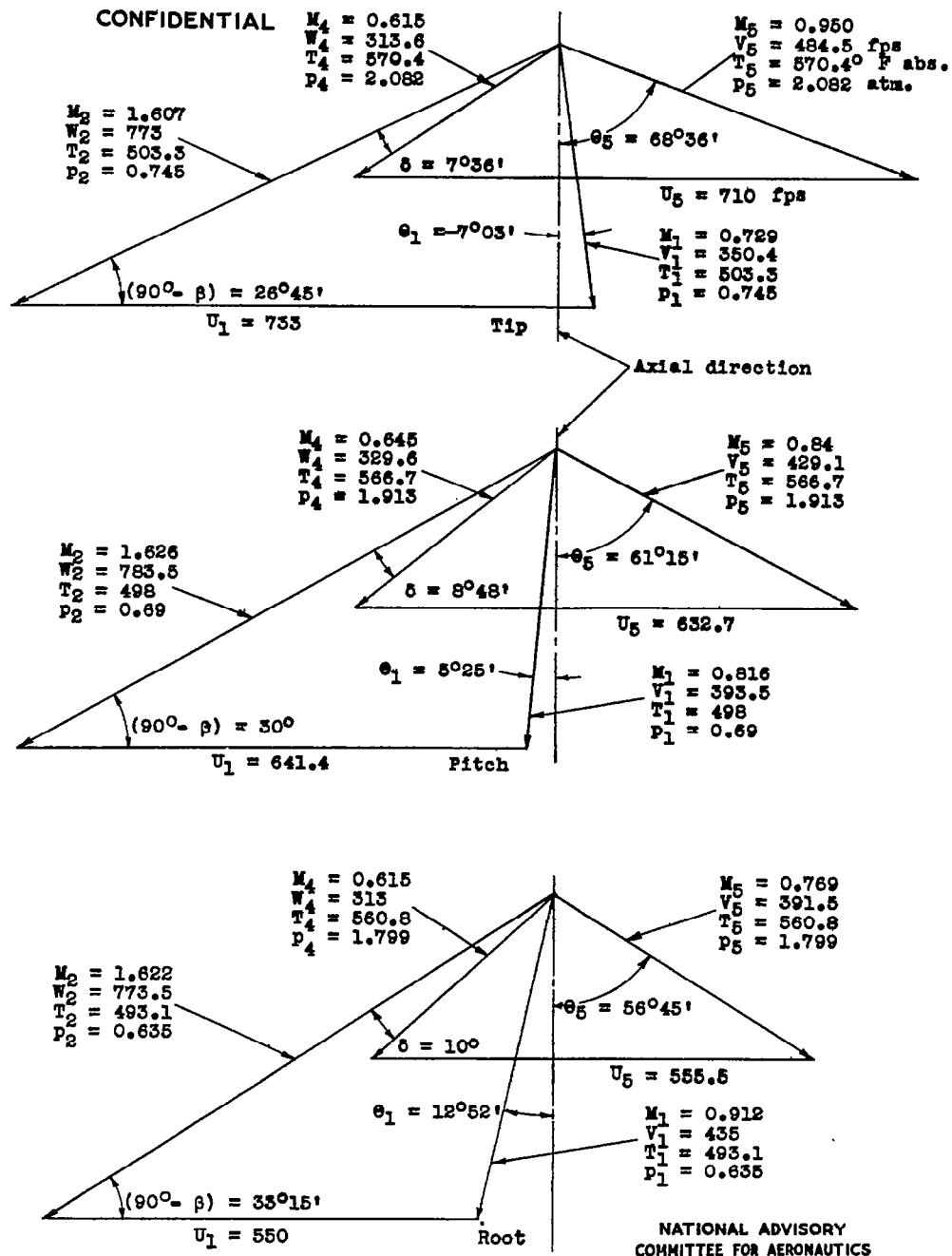


NATIONAL ADVISORY
COMMITTEE FOR AERONAUTICS

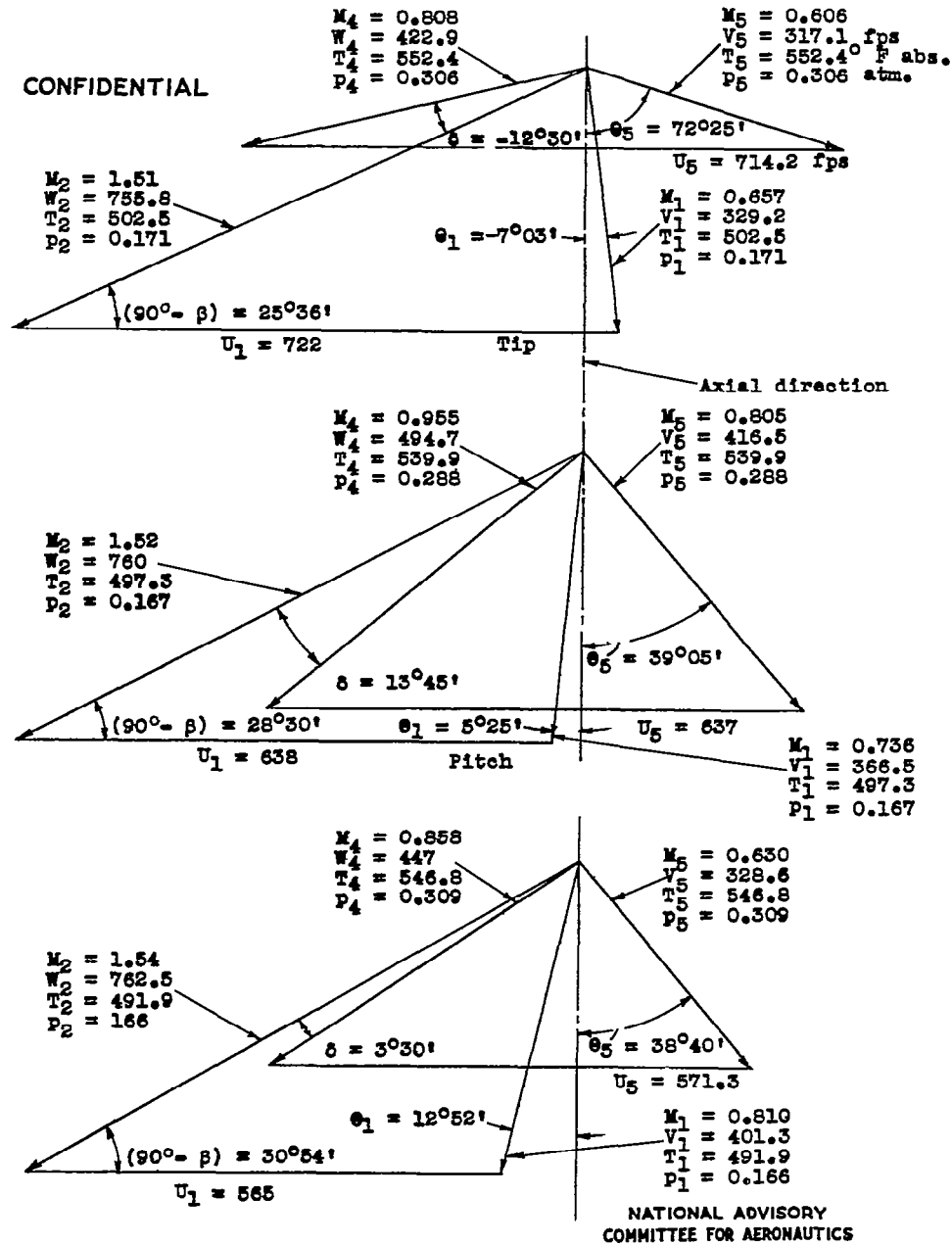
(b) Calculated velocity diagrams for the final test rotor in air, based on results of 1-inch-jet tests. Initial conditions: $p_0 = 1.00$ atmosphere; $T_0 = 520^\circ$ F absolute. Final weighted stagnation conditions: $T_{5s} = 719.1$; $\frac{P_5}{P_0} = 2.83$; and, with stator losses neglected, $\eta_r = 90.3$ percent.

Figure 2.- Continued.

CONFIDENTIAL



(c) Calculated velocity diagrams for the final test rotor in Freon-12 based on 1-inch-jet results, corresponding to the air diagrams in figure 2(b). Initial conditions: $p_0 = 1.00$ atmosphere; $T_0 = 520^\circ$ F absolute. Final weighted stagnation conditions: $T_{5s} = 591.5$; $\frac{P_5}{P_0} = 2.88$; and, with stator losses neglected, $\eta_p = 90.2$ percent.



(d) Velocity diagrams from data taken in actual tests at the design speed, $N = 10,500$ rpm, in Freon-12. Initial conditions: $p_0 = 0.225$ atmosphere; $T_0 = 515.8^\circ$ F absolute. Final weighted stagnation conditions: $\frac{P_5}{P_0} = 1.796$; the computed T_{5s} based on the pressure ratio, survey efficiency, and original stagnation temperature equals 561.2. For comparison, the measured T_{5s} (not accepted due to inconsistencies of thermocouple reading) equals 563. With stator losses neglected, $\eta_p = 80.6$ percent.

Figure 2.- Concluded.

CONFIDENTIAL

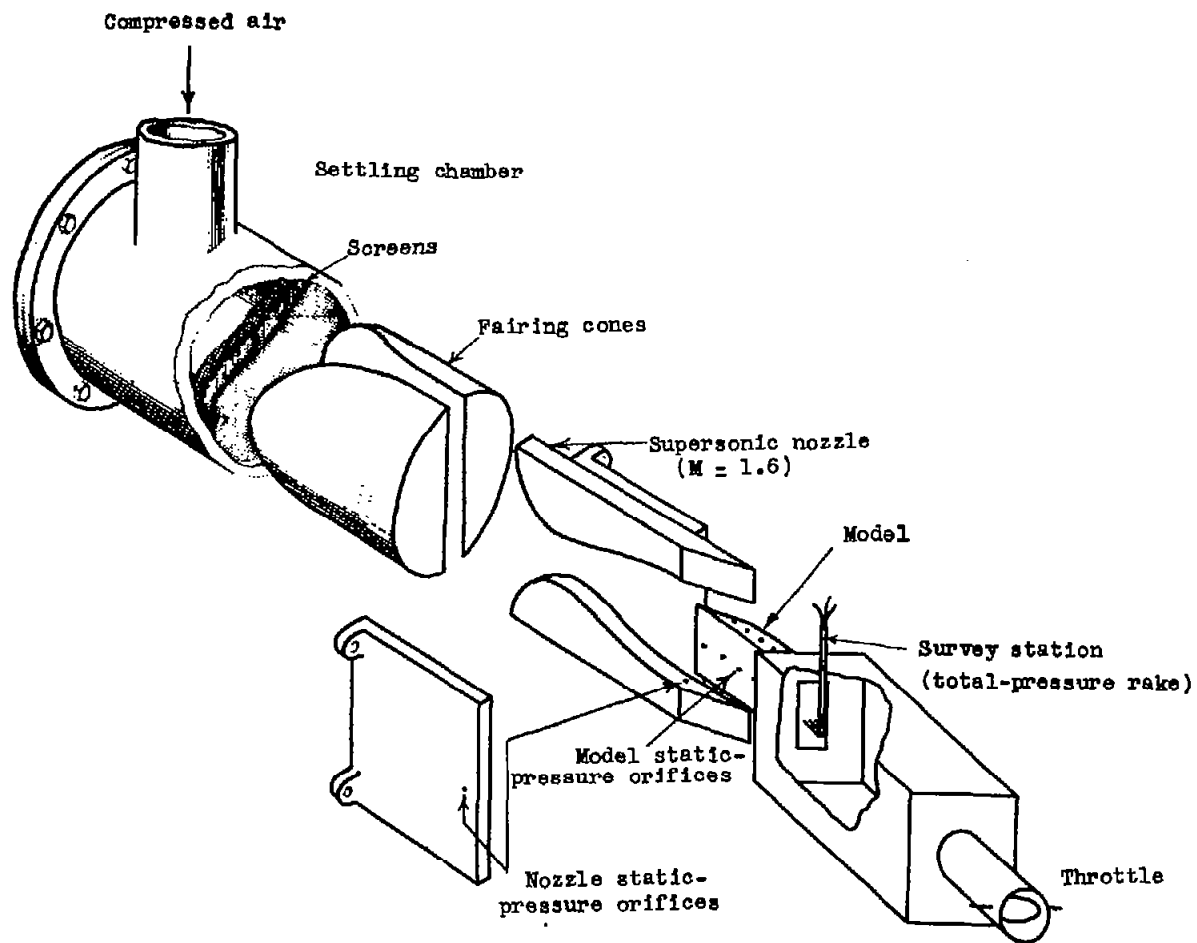


Figure 3.- Cut-away view of 1-inch jet showing installation of three-dimensional model. The survey was made by moving the total-pressure rake vertically at the station indicated.

NATIONAL ADVISORY
COMMITTEE FOR AERONAUTICS

CONFIDENTIAL

FIG. 3

NACA RM No. L6f01b

CONFIDENTIAL

NACA RM No. L6J01b

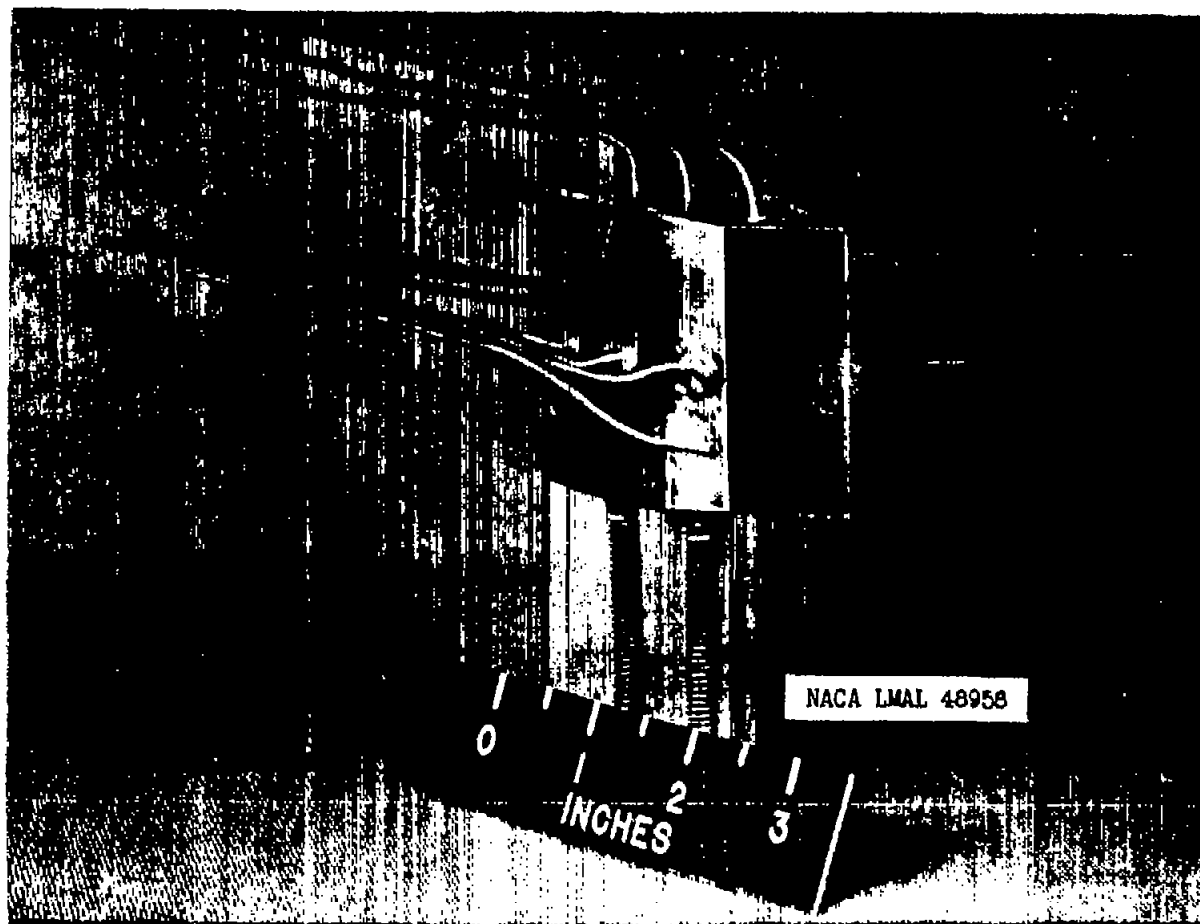


Figure 4.- Three-dimensional pressure-distribution model. The spill tube, located about $1/16$ inch from the leading edge and $1/16$ inch from the outer surface, and static orifices are shown. The total-pressure survey was taken directly behind the model. The outer surfaces do not represent the blades, and the model walls were thickened considerably.

Fig. 4

CONFIDENTIAL

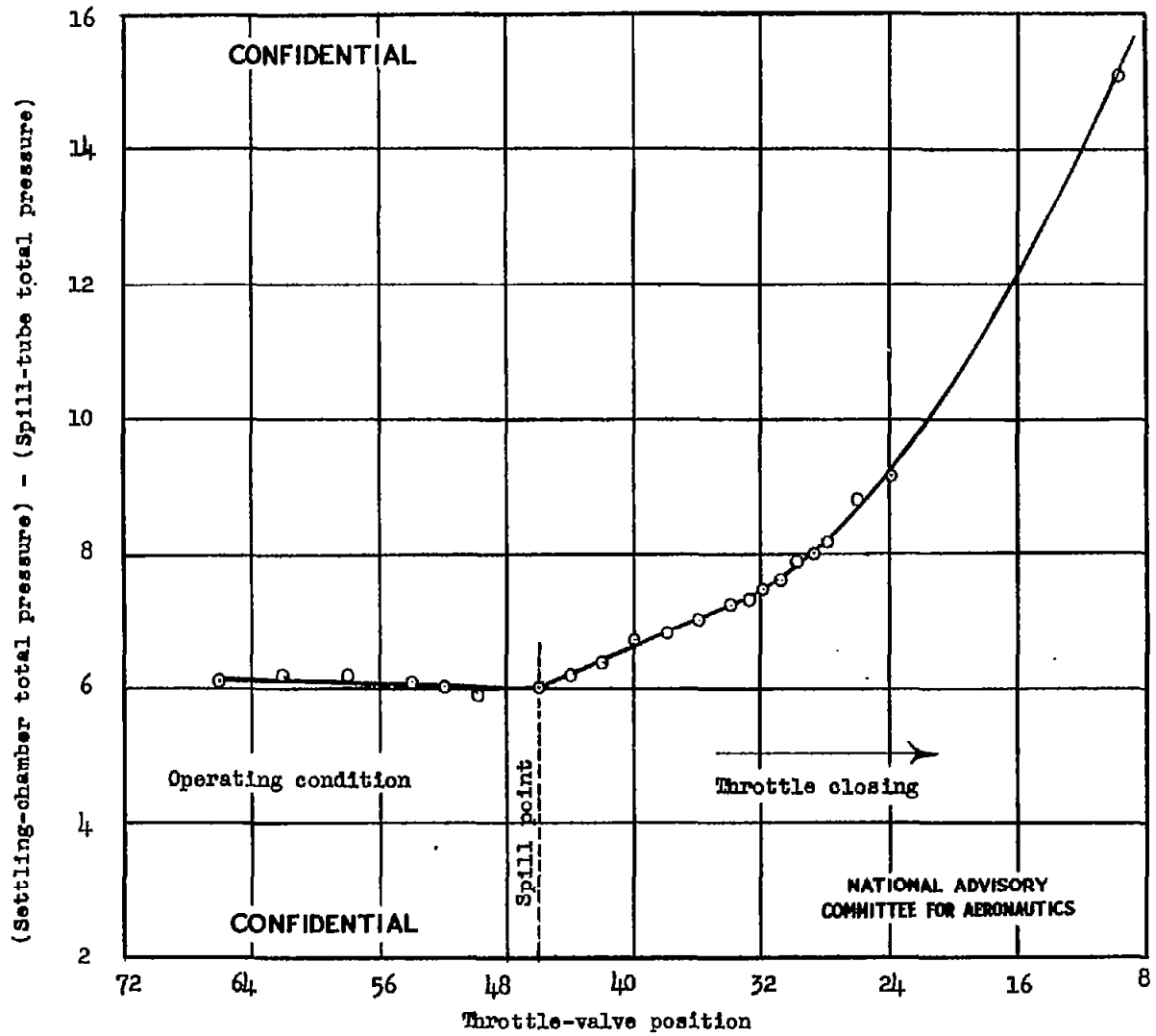
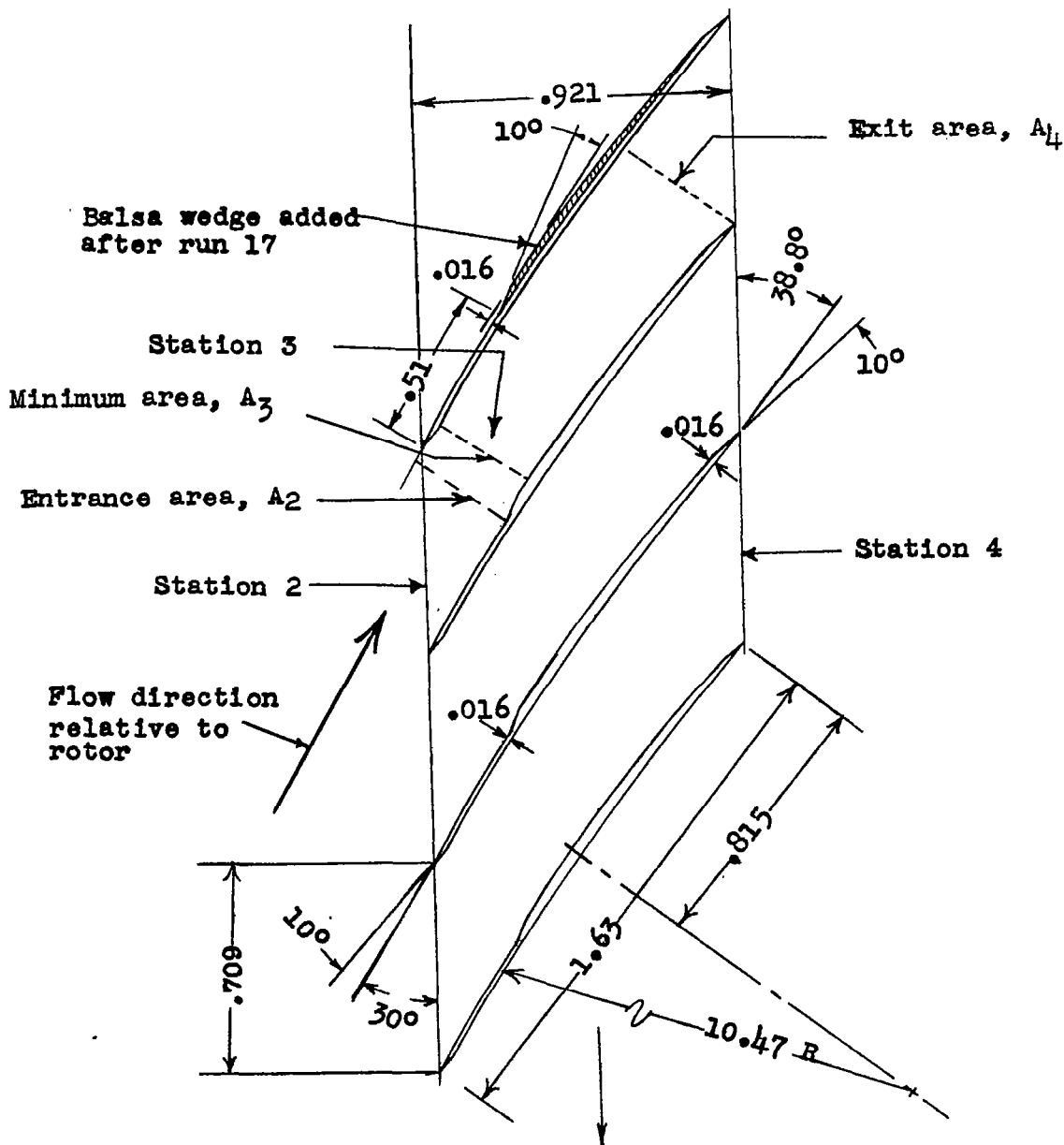


Figure 5.- Typical plot of spill-tube pressure against throttle-valve position showing location of spill point for 1-inch-jet model.

CONFIDENTIAL



NATIONAL ADVISORY
COMMITTEE FOR AERONAUTICS

Figure 6.- Cross section through rotor blades at 14-inch (pitch) diameter. Design configuration; 62 blades used. (All dimensions are in inches.)

CONFIDENTIAL

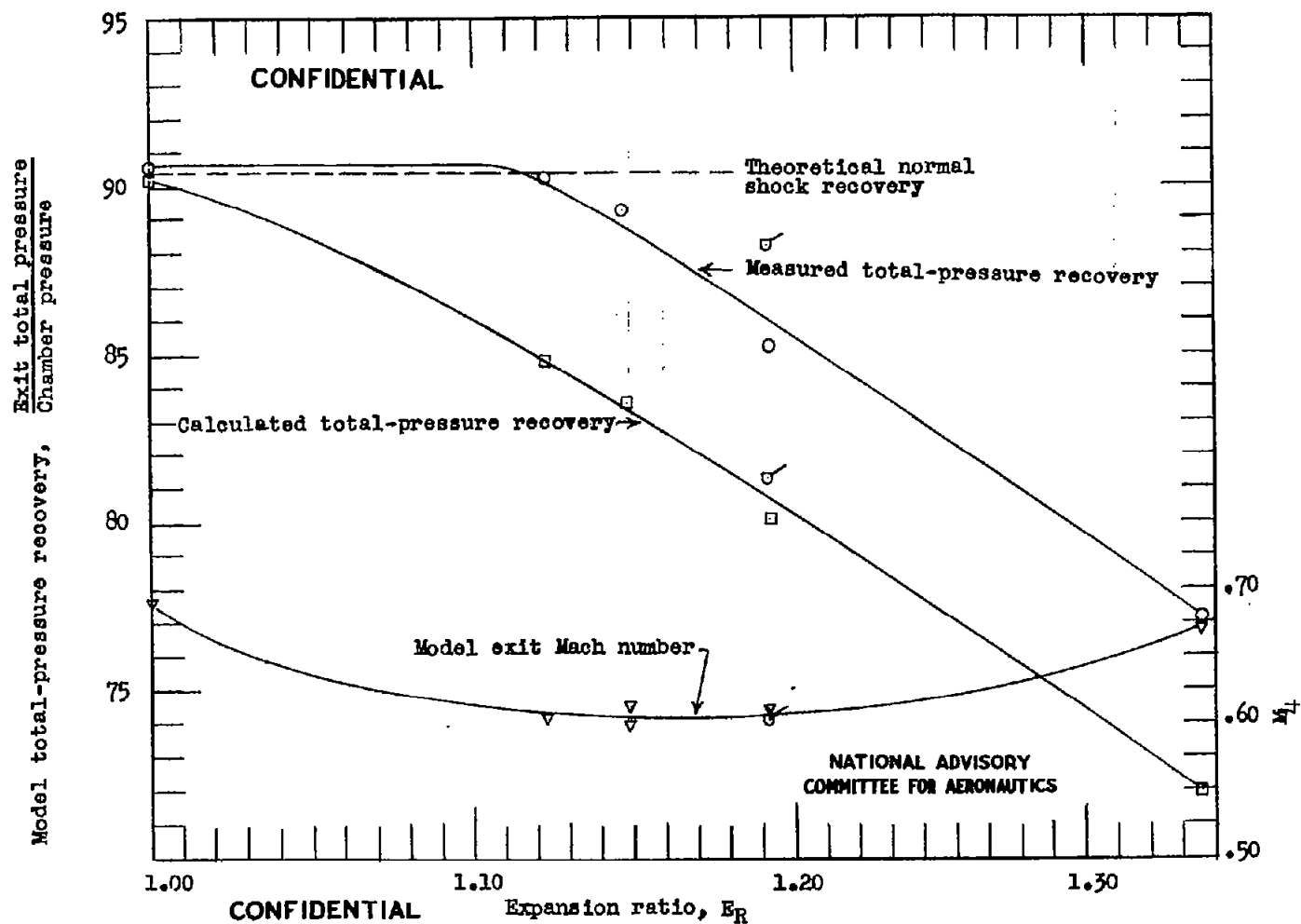
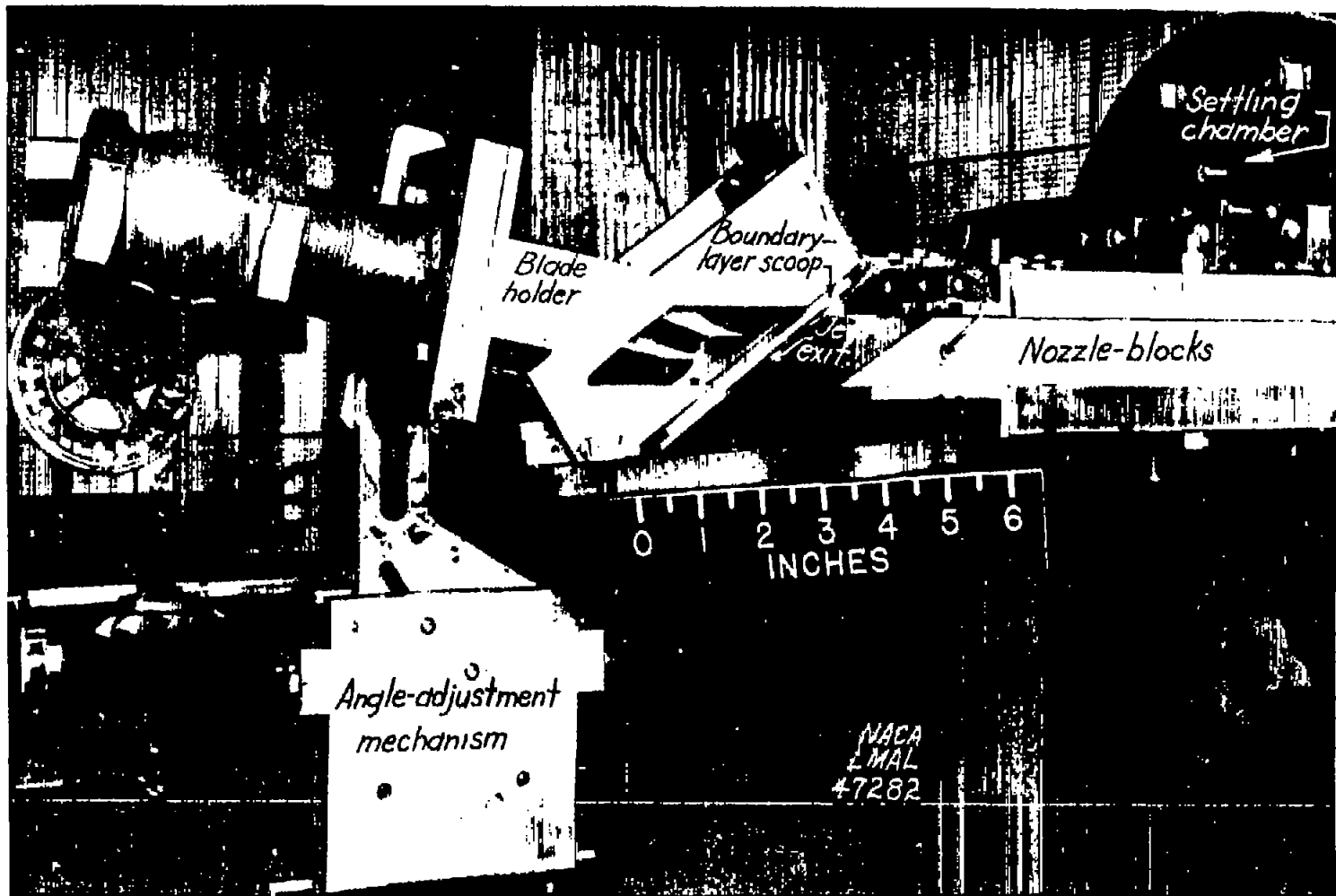


Figure 8.- Measured total-pressure recovery, calculated total-pressure recovery, and exit Mach number variation with expansion ratio for 1-inch-jet blade model. Data taken at spill point; model entrance Mach number, $M_2 = 1.58$. ($C_R = 1.042$ except for flagged symbols where $C_R = 1.092$.)

CONFIDENTIAL



NACA RM No. L6f01b

Figure 9.- Setup for schlieren photography. The throttling valve for regulation of back pressure is located on the left and the 1-inch-jet nozzles are shown at the right. In the center a model may be seen through the glass side walls.

Fig. 9

CONFIDENTIAL



(a)

Strong oblique shock from 10°
leading-edge angle (Fig. 6)



(e)

Flow direction



Weak shock from (b)
leading edge



Transonic region

(f)

Model leading edges



(c)



Jet exit

(g)



(d)

NACA LMAL 48948



(h)

Figure 10.- Schlieren sequence showing the flow process and characteristics as the model back pressure is progressively increased. Photograph (a) shows the unthrottled flow with the shock in back of the model. Photograph (h) shows the shock pushed completely outside of the model as an unattached bow wave. The design operating condition appears to be that shown in photograph (f).

CONFIDENTIAL

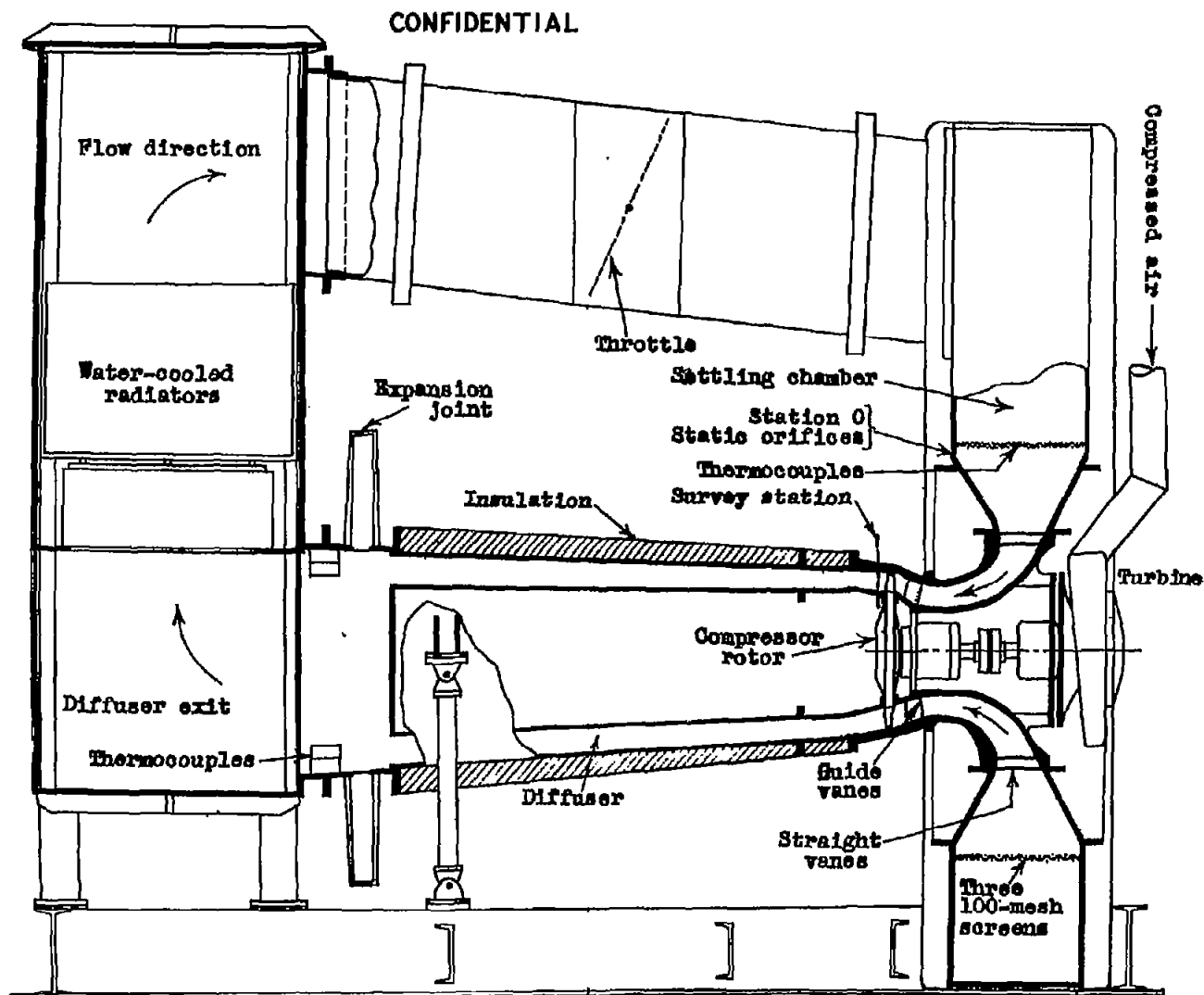


Figure 11.- Sectional view of the supersonic-compressor test setup.

NATIONAL ADVISORY
COMMITTEE FOR AERONAUTICS

CONFIDENTIAL

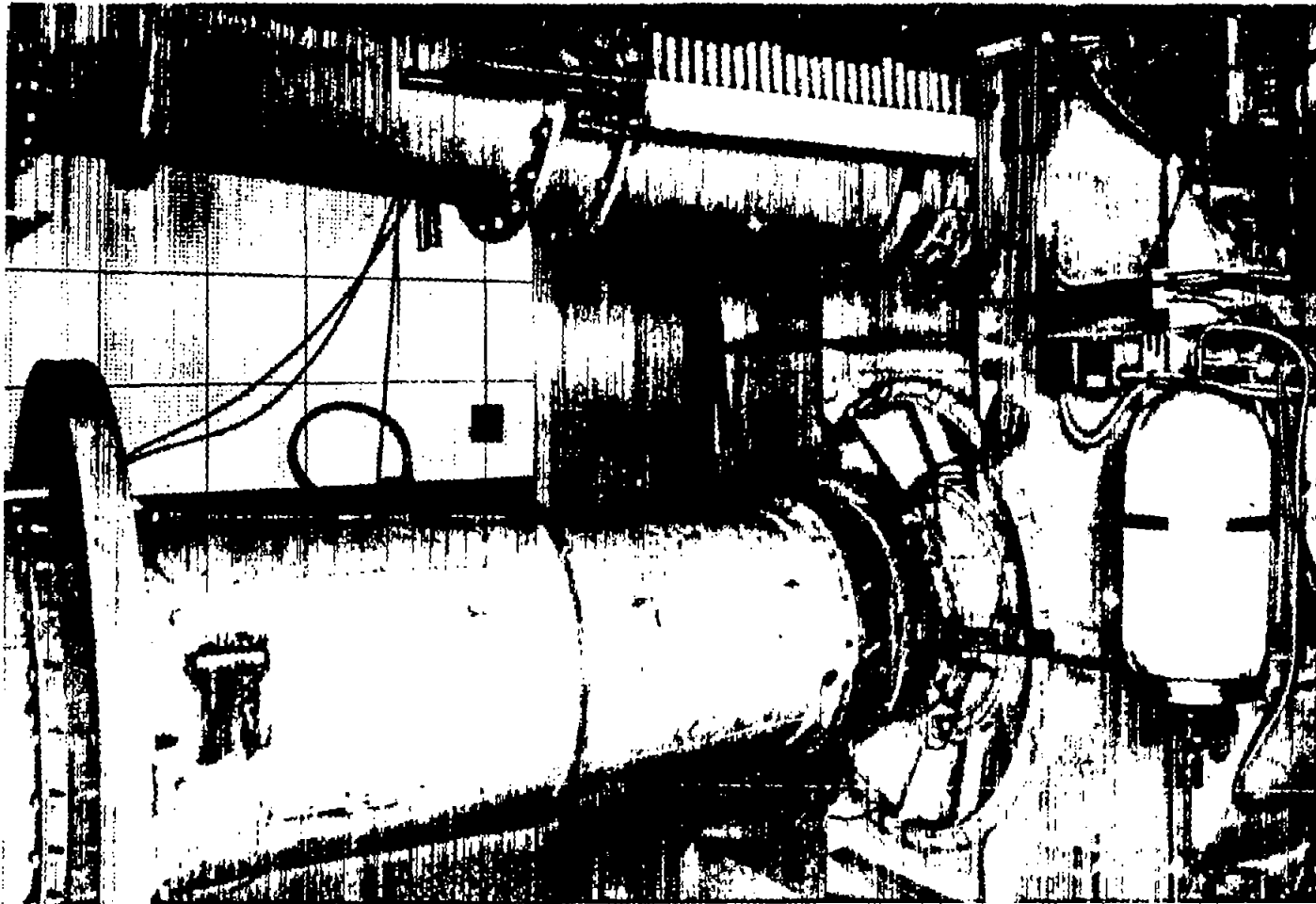


Figure 12.- Supersonic-compressor test setup. The throttling-valve lever and protractor are visible on the upper return section. The velocity-of-sound meter for determining the composition of the test fluid is shown at the upper right.

CONFIDENTIAL

NACA RM No. L6F01b

Fig. 12

CONFIDENTIAL

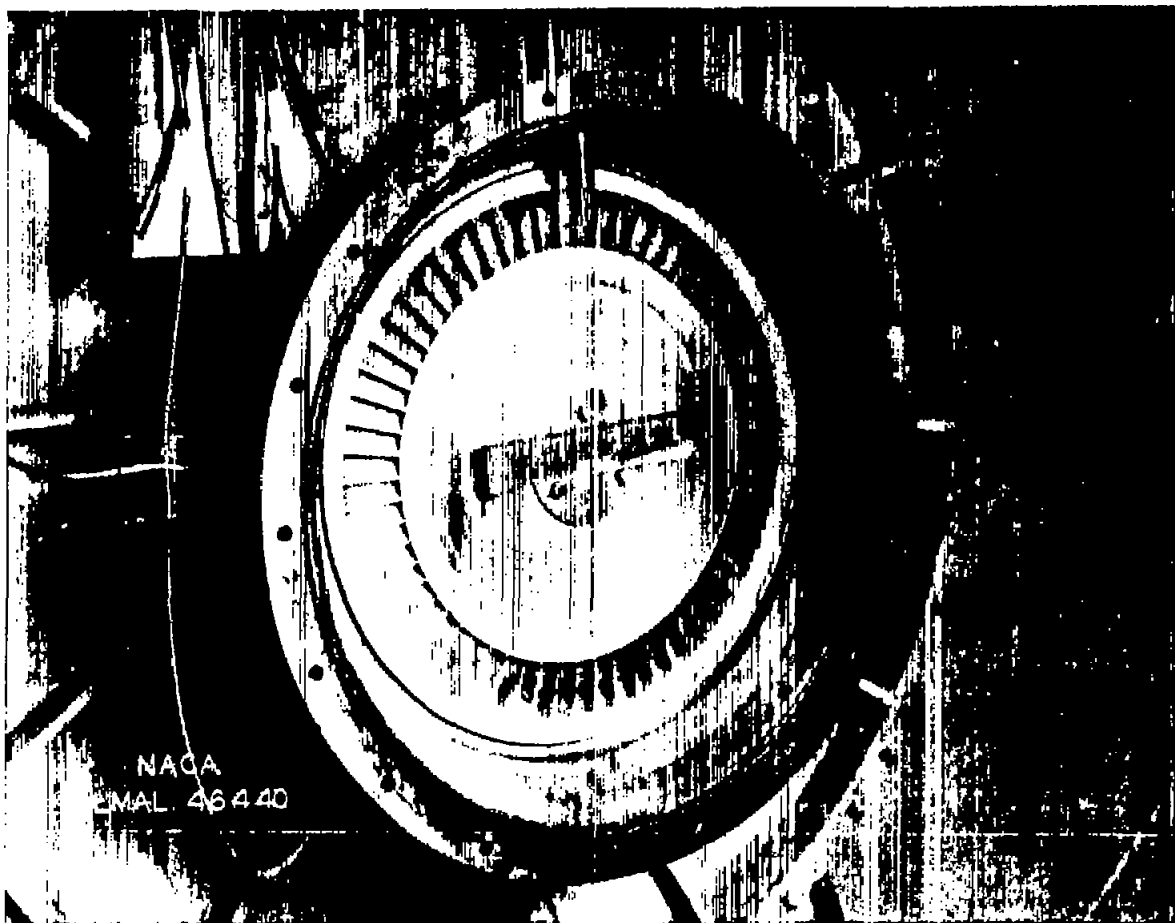


Figure 13.- Downstream view of the rotor showing the survey-instrument location and the balsa-wood inserts beneath the shroud. The cylindrical surfaces which form the aerodynamic passages following the rotor have been removed.

CONFIDENTIAL

NACA RM No. L6701b

Fig. 13

CONFIDENTIAL

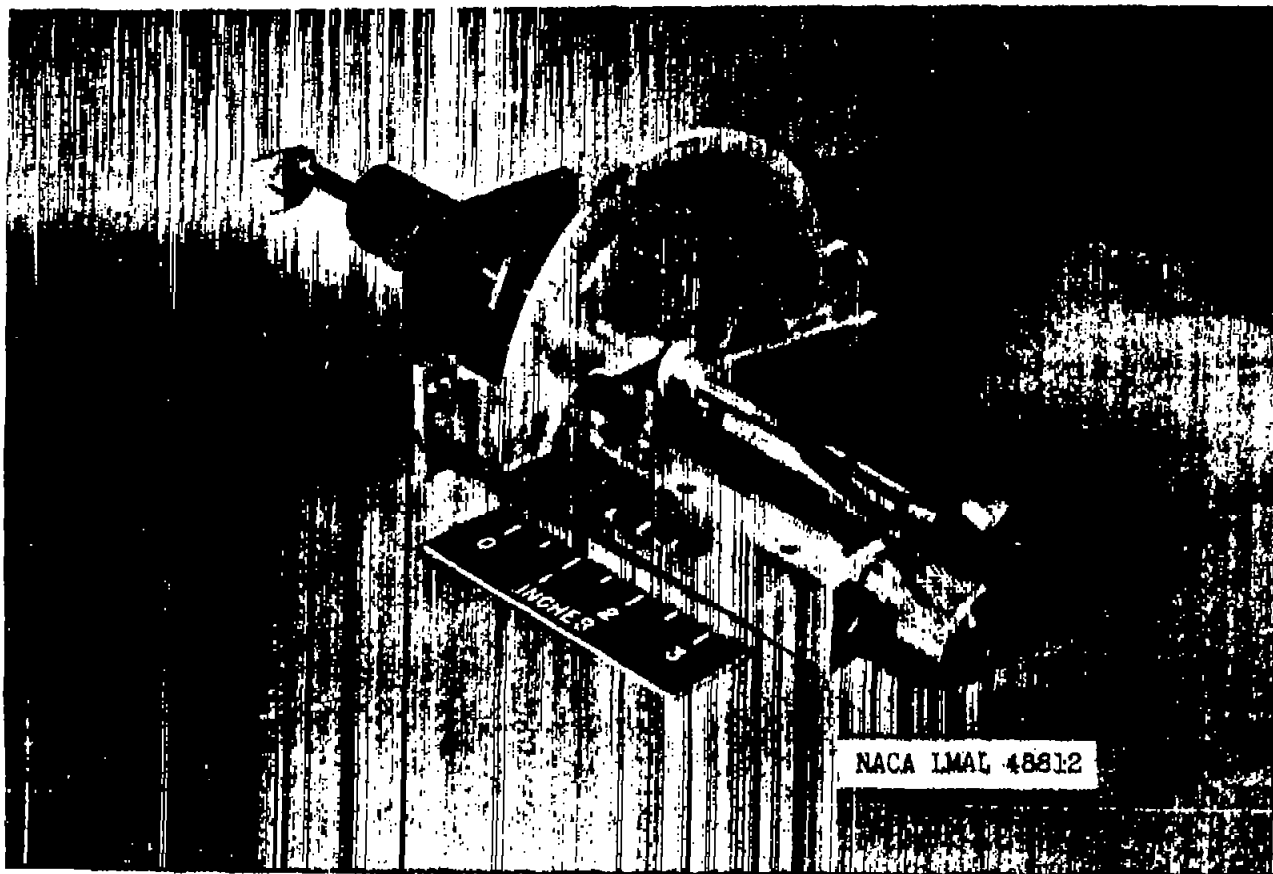


Figure 14.- Survey instrument for supersonic-compressor test. Instrument contains total-pressure tube (short tube), a static-pressure tube (long tube), and a null type yawmeter (center). (The scale indicating the radial position of the instrument is visible, as are the protractor and vernier arm.)

CONFIDENTIAL

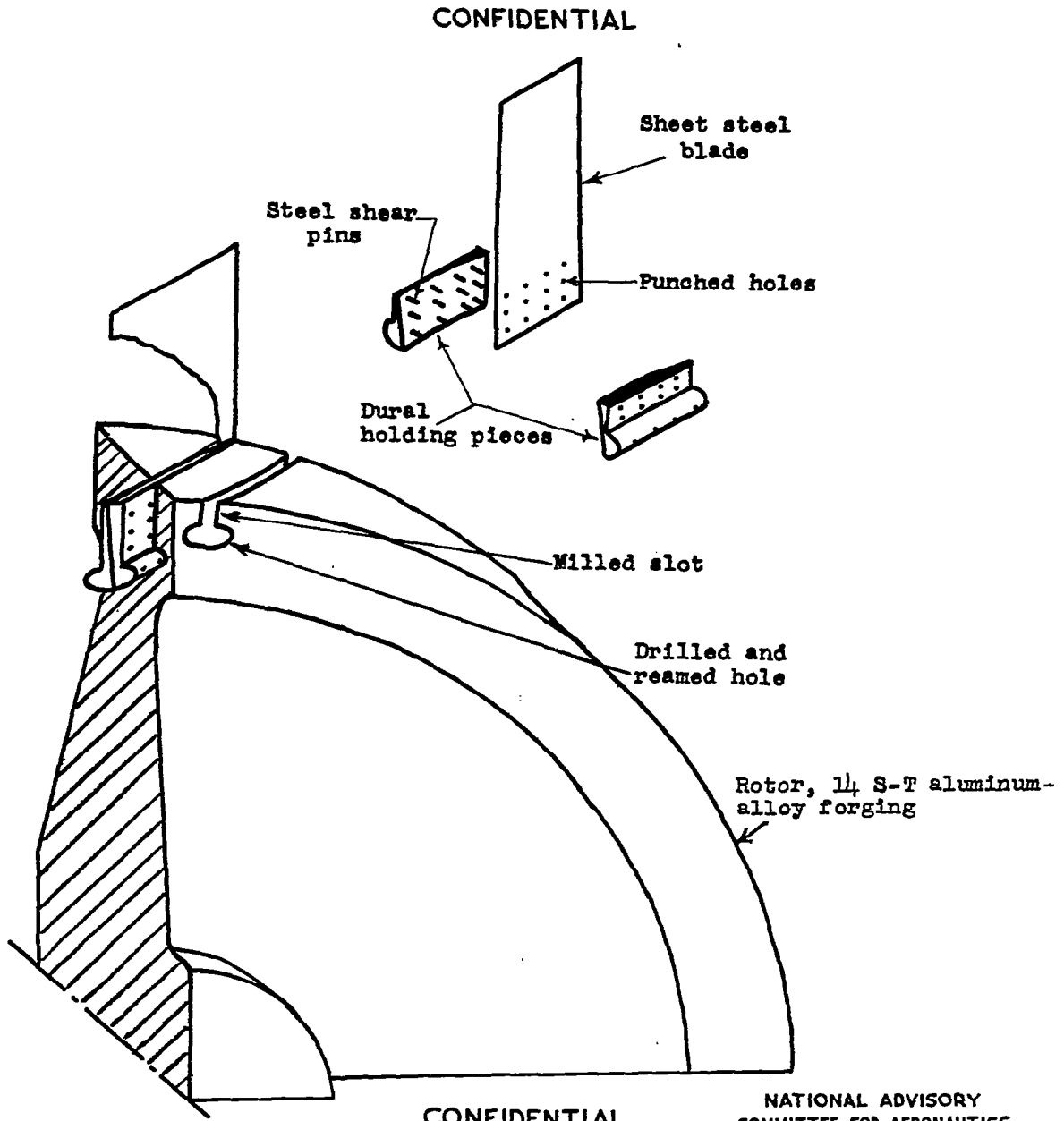


Figure 15.- Schematic drawing showing blade-attachment method.

CONFIDENTIAL

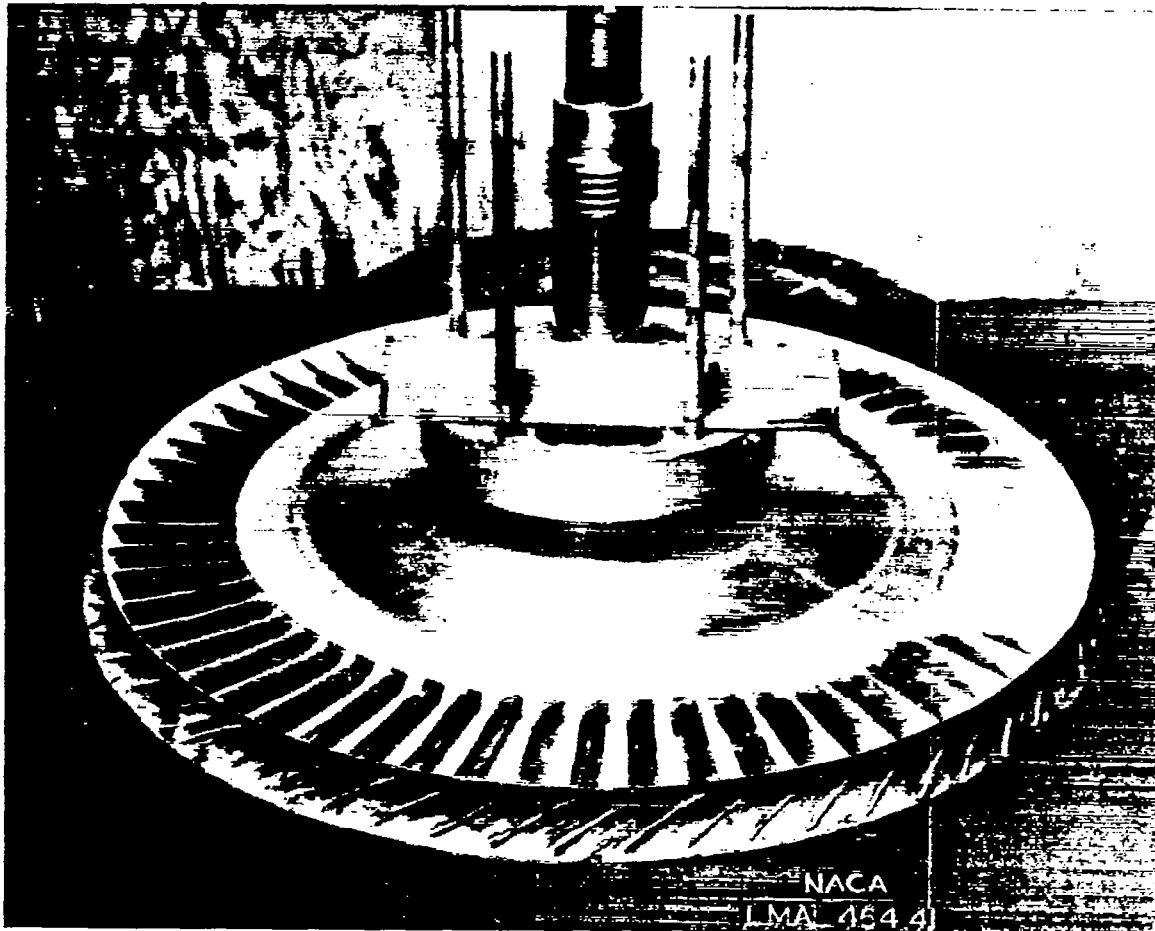


Figure 16.- Supersonic-compressor rotor and shaft. Lacquered balsa-wood inserts are shown on the rearward side of each blade. The blade-tip curvature may be seen on the outside of the shroud. The curvature is completely washed out at the blade pitch sections.

CONFIDENTIAL

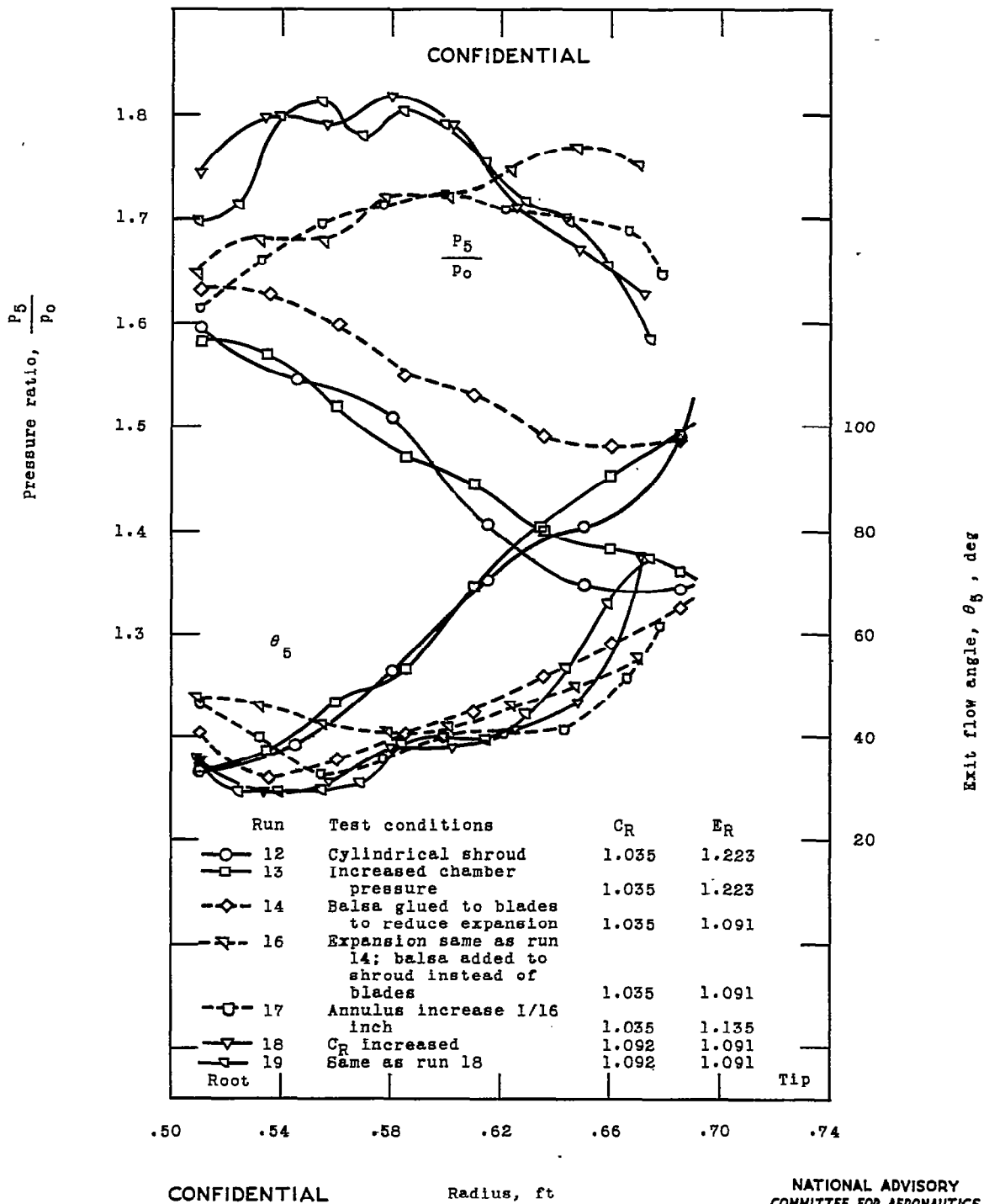
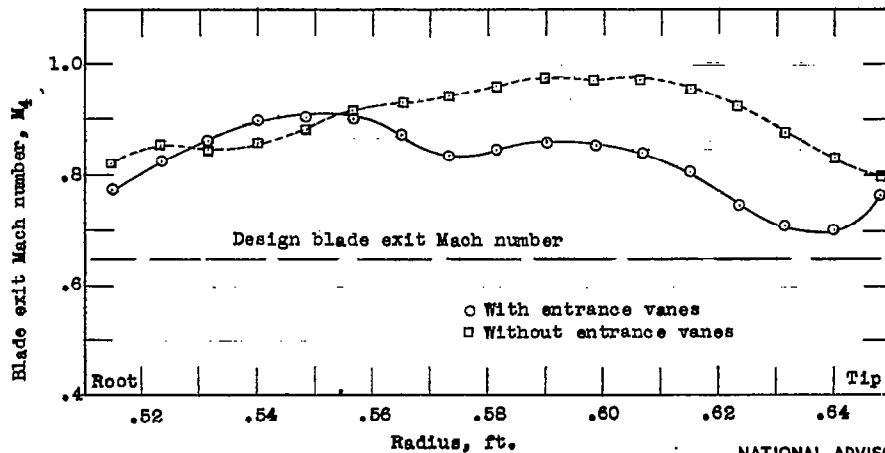
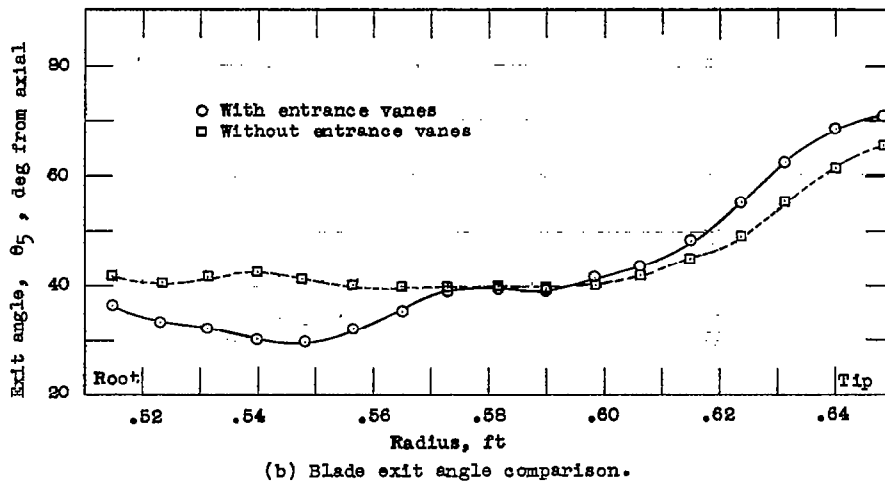
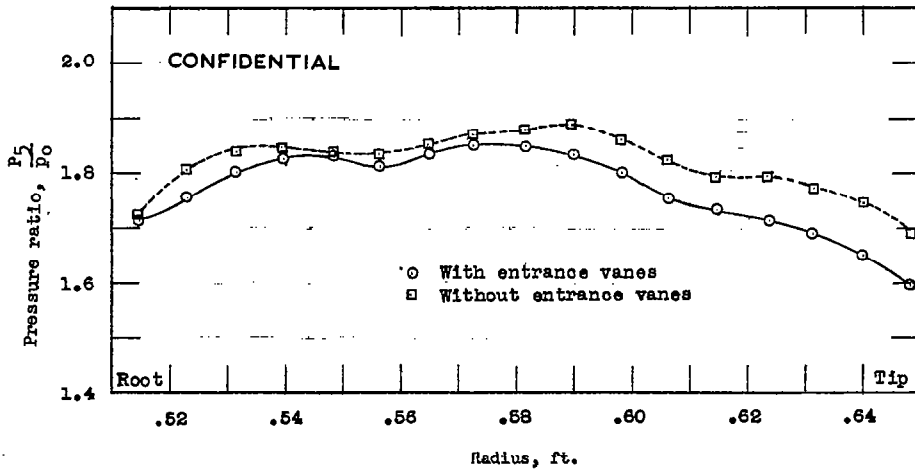


Figure 17.- Variation of total-pressure ratio and exit flow angle over rotor exit annulus for early exploratory tests. Rotational speed, 10,000 rpm.



CONFIDENTIAL

(c) Blade exit Mach number comparison.

NATIONAL ADVISORY
COMMITTEE FOR AERONAUTICS

Figure 18.- Comparisons of a typical run with and without entrance vanes. Survey points are plotted for the blade-exit annulus; N , 10,500 rpm; $M_0 = 1.4$. It can be seen that the flow at the tip was improved somewhat by omitting the entrance vanes ahead of the rotor.

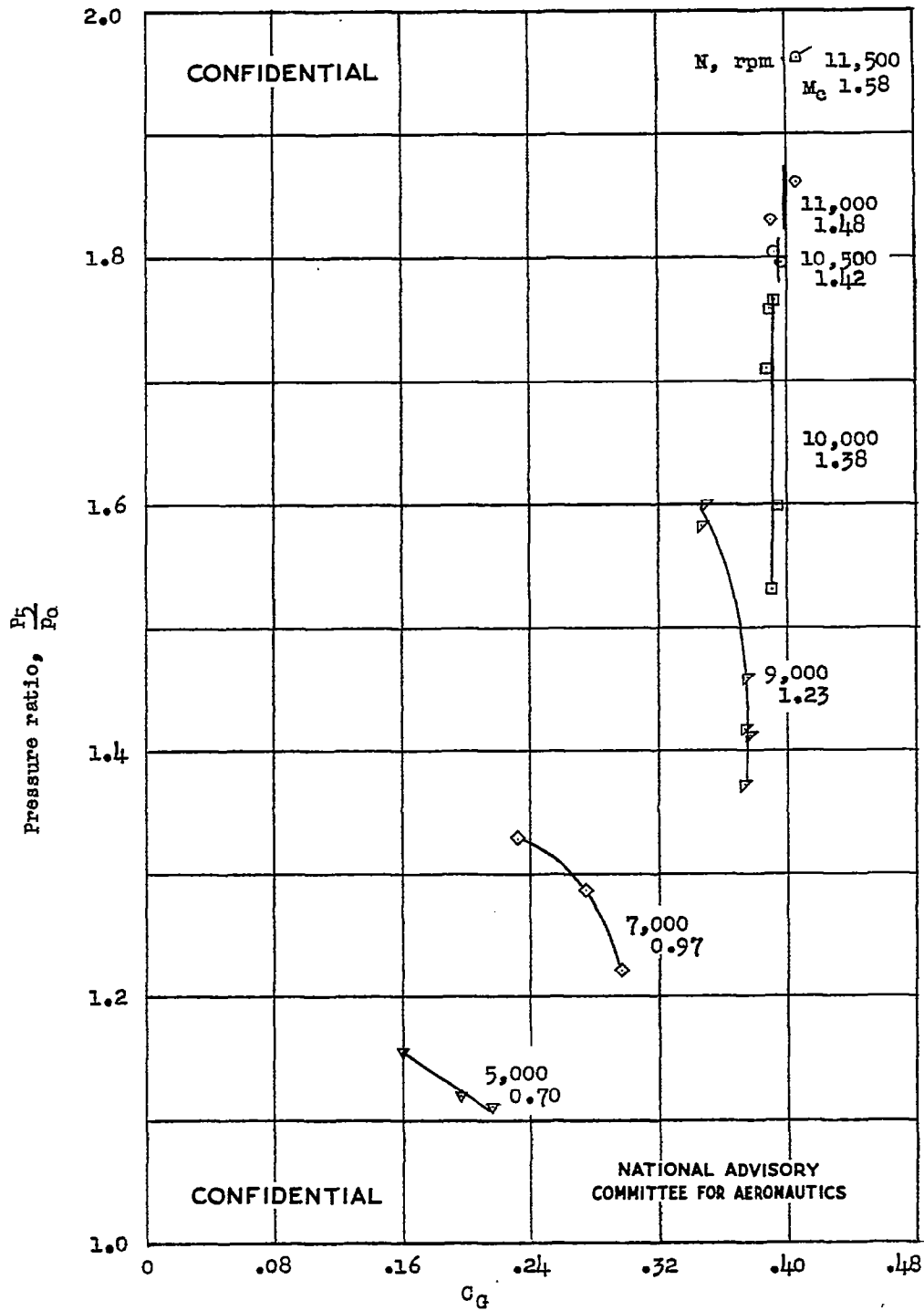


Figure 19.- Variation of mass-flow coefficient C_G with throttling and compressor Mach number. These data were obtained from surveys behind the rotor and therefore do not include any stator losses. (Flagged symbols represent 12-point survey test.)

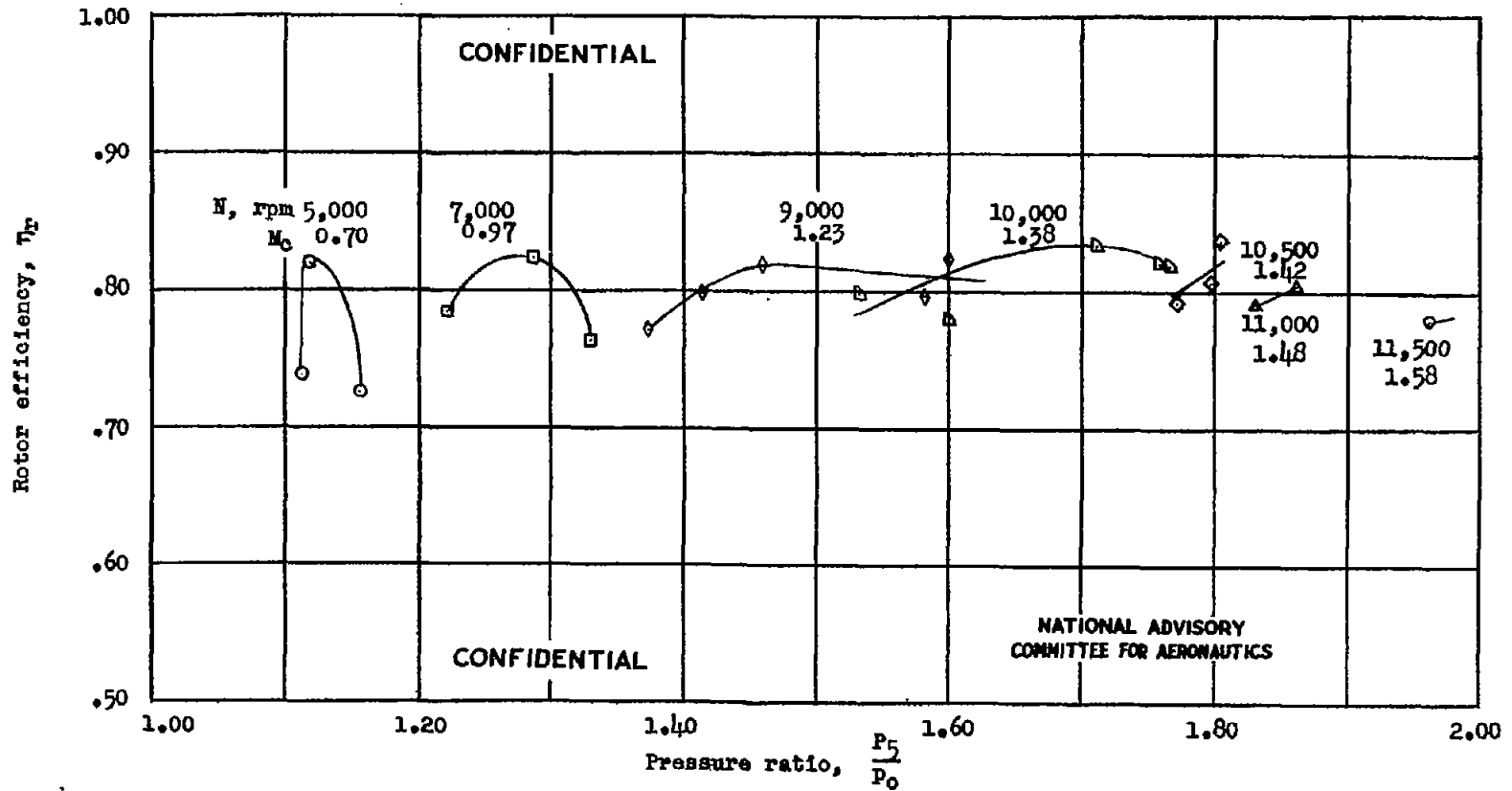


Figure 20.- Efficiency variation with throttling and compressor Mach number. (Flagged symbol represents 12-point survey.) Data are from surveys in Freon-12 behind the rotor and do not include stator losses.

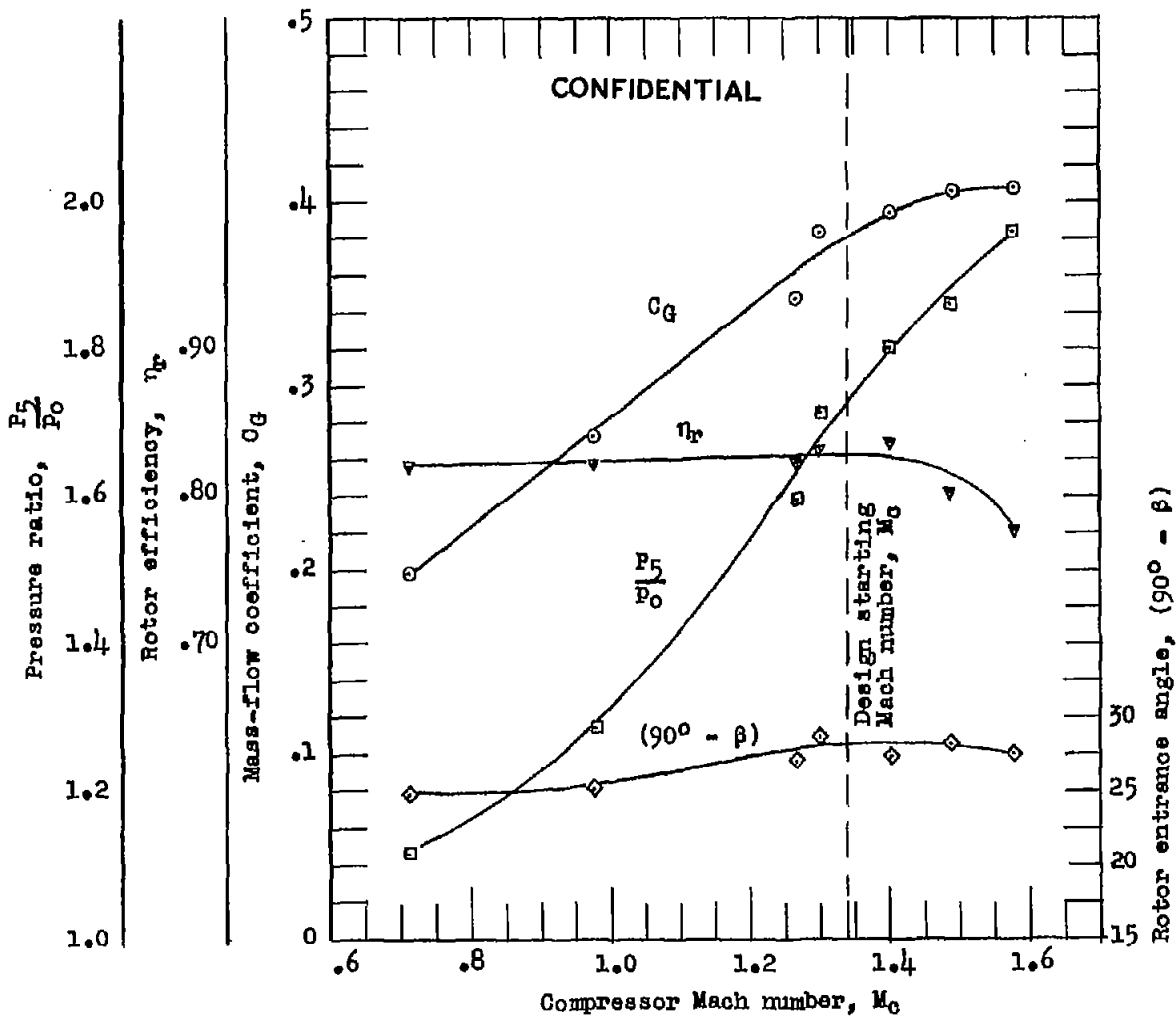


Figure 21.- Variation of peak efficiency characteristics with compressor Mach number. The efficiencies and pressure ratios are based on surveys behind the rotor and do not include any stator losses.

NATIONAL ADVISORY
COMMITTEE FOR AERONAUTICS

CONFIDENTIAL

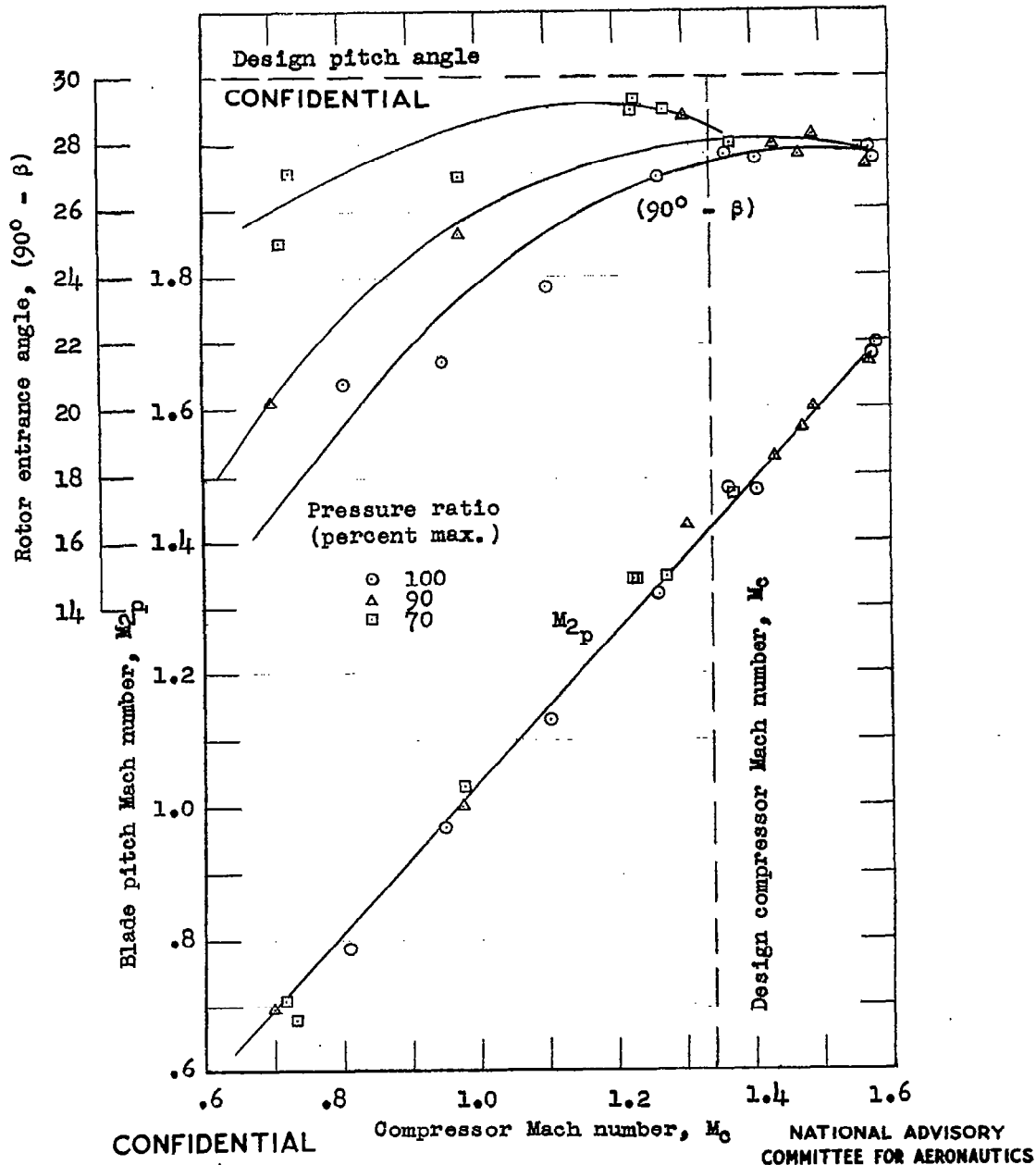


Figure 22.- Angle of flow $(90^\circ - \beta)$ and blade pitch Mach number M_{2p} entering rotor at the pitch diameter against compressor Mach number M_c . For M_{2p} greater than about 1.53 (the design starting blade Mach number), the entrance angle is shown to be independent of throttle position as would be expected from the theory of the supersonic operating range. It is to be noted that in Freon-12, at the design value of $M_c = 1.43$, the value of $M_2 = 1.53$, whereas in air $M_2 = 1.62$. (See appendix D.)